

4. EXPLANATORY NOTES¹

Shipboard Scientific Party²

INTRODUCTION

In this chapter, we have assembled information that will help the reader to understand the observations on which our preliminary conclusions have been based and also to help the interested investigator select samples for further analysis. This information concerns only shipboard operations and analyses described in the site reports in the *Initial Reports* volume of the Leg 156 *Proceedings of the Ocean Drilling Program*. Methods used by various investigators for shore-based analyses of Leg 156 data will be described in the individual scientific contributions to be published in the Leg 156 *Scientific Results* volume.

Authorship of Site Chapters

The separate sections of the site chapters were written by the following shipboard scientists (authors are listed in alphabetical order, no seniority is implied):

Site Summary: Ogawa, Shipley
Background and Objectives: Ogawa, Shipley
Operations: Blum, Fisher, Foss, Meyer, Ogawa, Shipley
Lithostratigraphy and Sedimentology: Jurado, Meyer, Underwood
Structural Geology: Housen, Labaume, Leitch, Maltman, Tobin
Biostratigraphy: Steiger, Xu
Paleomagnetism: Housen
Organic Geochemistry: Laier
Inorganic Geochemistry: Kastner, Zheng
Core Physical Properties: Ashi, Blum, Brückmann, Henry, Peacock
Downhole Logging: Filice, Fisher, Goldberg, Jurado, J.C. Moore, G. Moore, Yin, Zwart
In Situ Temperature Measurements: Fisher
Vertical Seismic Profiling: G. Moore, Peacock
Packer Flow Tests: Fisher
Summary and Conclusions: Ogawa, Shipley

Following the site chapters are summary core descriptions ("barrel sheets") and photographs of each core.

ODP is in the process of replacing the bulk of the "Explanatory Notes" chapters in each *Initial Reports* volume with an annual "Explanatory Notes" chapter to *Initial Reports* volumes. These complete, detailed, and annually updated notes will reduce redundancy, maintain completeness and quality, and help to reduce printing costs of *Initial Reports* volumes. In anticipation of this change, we have omitted some of the general information that has been reprinted repeatedly in past *Initial Reports* volumes and kept the notes as short as possible. Reference is made to other *Initial Reports* volumes and to the ODP Technical Notes series for detailed description of methods, if appropriate.

Drilling, Coring, and Casing Operations

During Leg 156, use was made for the first time in scientific ocean drilling history of logging-while-drilling (LWD) tools. LWD drilling (and simultaneous measurement of resistivity, bulk density, neutron porosity, and spectral gamma ray with two instrumented drill collars leased from Anadrill) for the first five days of the cruise preceded coring and other downhole experiments. It provided an excellent database for operational and scientific decisions during the remainder of the cruise (see "Downhole Logging" sections, this chapter, and "Operations" and "Downhole Logging" sections in site chapters).

Coring was performed with three systems during Leg 156: the advanced hydraulic piston corer (APC), the extended core barrel (XCB), and the rotary core barrel (RCB). These systems were applied to maximize core recovery in the lithology being drilled and for hole stability requirements. Coring systems and their characteristics, such as drilling-related deformation, are eloquently summarized in the "Explanatory Notes" chapter of the Leg 139 *Initial Reports* volume, and various versions can be found in various *Initial Reports* volumes.

The Leg 156 coring program was limited in the interest of downhole experiments and deployment of instrumented borehole seals through the décollement. The APC was used only for mud-line core to determine depths of the seafloor at each site. Coring then proceeded from about 100 m above the décollement to about 50 m below the décollement with the XCB. Core recovery over these intervals varied from excellent to very poor, while the quality of the cores suffered moderately to severely from "biscuiting," a typical drilling disturbance with the XCB.

Leg 156 championed an ambitious borehole casing program that allowed for deployment of instrumented borehole seals and vertical seismic profiling (VSP) experiments and packer flow tests. For the first time, ODP used triple (16-, 13³/₈-, and 10³/₄-in.) casing strings, mud motor, and underreamers to enlarge the hole while setting the third casing, and a wire-screened interval to allow for packer flow tests in the lowermost, unstable formation. A record length of 476 m of 13³/₈-in. casing was set in Hole 948D.

Special Downhole Experiments and CORK Deployment

The primary goal of Leg 156 was the deployment of borehole seals with instrumented cables extending down to the bottom of the hole for long-term monitoring of temperature and pressure (see "Borehole Seals and Long-Term Measurements" section, this chapter). To calibrate and compare long-term temperature variations with conditions before drilling the hole, numerous in situ temperature measurements were performed with the water sampler temperature probe (WSTP). Packer tests in the lowermost parts of two holes, cased with a screened interval, provided estimates of in situ permeability (see "Packer Flow Tests" sections, this chapter and other site chapters).

Shipboard Procedures for Core Analyses

General core-handling procedures have been described in previous *Initial Reports* volumes and in the *Shipboard Scientist's Handbook* and are summarized here. As soon as cores arrived on deck, core-catcher samples were taken for the biostratigraphic laboratory,

¹ Shipley, T.H., Ogawa, Y., Blum, P., et al., 1995. *Proc. ODP, Init. Repts.*, 156: College Station, TX (Ocean Drilling Program).

² Shipboard Scientific Party is as given in list of participants preceding the contents.

and gas samples were taken immediately for analysis as part of the shipboard safety and pollution prevention program. When the core was cut in sections, whole-round samples were taken for shipboard interstitial water analyses, and headspace gas samples were immediately scraped from the ends of cut sections and sealed in glass vials for light-hydrocarbon analysis.

Core sections then arrived in the core laboratory, where their depths and lengths were recorded and the "Corelog" was produced. The numbering of sites, holes, cores, and samples followed the standard ODP procedures. A complete identification number for a sample consists of the following information: leg, site, hole, core number, core type, section number, piece number (for hard rock), and interval in centimeters, measured from the top of the section. For example, a sample identification of "156-948C-10X-1, 10-12 cm" would be interpreted as representing a sample removed from the interval between 10 and 12 cm below the top of Section 1, Core 10 (X designates that this core was taken with the XCB system) of Hole 948C during Leg 156.

Cored intervals are referred to in meters below seafloor (mbsf); these are determined by subtracting the height of the rig floor above sea level (as determined at each site) from the drill-pipe measurements from the drill floor. Note that this measurement usually differs from precision depth recorder (PDR) measurements by a few to several meters. Because Core 156-949B-14X had 197% recovery, an alternative method for determining "corrected" subseafloor depths (in mbsf) was devised; this method is described in the "Operations" section of the "Site 949" chapter (this volume).

After whole-round sections were run through the multisensor track (MST; see "Physical Properties" section, this chapter) and thermal conductivity measurements were performed, additional whole-round samples were taken for shore-based fabric, permeability, and acoustic tests under varying effective stresses. The cores were subsequently split into working and archive halves. Cores were split from the bottom to top, so investigators should be aware that older material could have been transported upward on the split face of each section. The working half of each core was sampled for both shipboard and shore-based laboratory studies, while the archive half was described visually and by means of smear slides. Thin sections were taken from the working half. Most archive sections were run through the cryogenic magnetometer. The archive half was then photographed with both black-and-white and color film, a whole core at a time, and close-up photographs (black and white) were taken of particular features for illustrations in the summary of each site, as requested by individual scientists.

Both halves of the core then were placed into labeled plastic tubes, sealed, and transferred to cold-storage space aboard the drilling vessel. At the end of the cruise, the cores were transferred from the ship into refrigerated trucks and to cold storage at the Bremen Core Repository of the Ocean Drilling Program, in Bremen, Federal Republic of Germany.

LITHOSTRATIGRAPHY AND SEDIMENTOLOGY

Sediment "Barrel Sheets"

Core description forms, or "barrel sheets," summarize the data obtained during shipboard analysis of each sediment core. Shipboard sedimentologists were responsible for visual core logging, smear slide analyses, and thin section descriptions. Detailed observations at the section scale were recorded initially by hand on standard ODP Visual Core Description (VCD) forms. Structural geologists recorded deformation features on VCD forms of their own design (see "Structural Geology" section, this chapter). Copies of the Visual Core Descriptions are available from ODP on request.

Core Designation

Core designations include the leg, site, hole, core number, and core type, as discussed in a preceding section (see "Numbering of

Sites, Holes, Cores, and Samples" in "Introduction" section, this chapter). Each cored interval is specified in terms of meters below seafloor (mbsf).

Graphic Lithology Column

As many as three graphic patterns appear on the core description forms for each lithology within the column titled "Graphic Lithology" (Fig. 1). For intervals containing homogeneous mixtures of sediment or sedimentary rock, the constituent categories are separated by solid vertical lines; each category is represented by its own pattern and average abundance. Where intervals constitute two or more sediment lithologies having different compositions (e.g., thinly bedded or highly variegated sediments), average abundances of the lithologic constituents are represented by dashed vertical lines. The "Graphic Lithology" column shows only intervals that exceed 20 cm in thickness. Some constituents account for <10% of a given lithology; others remain after the three most abundant lithologies have been represented in the "Graphic Lithology" column. These types of materials are listed in the "Description" section of the core description form.

Age Column

Chronostratigraphic position, as defined by paleontological and paleomagnetic criteria, is shown in the "Age" column on the core description forms. Sharp boundaries are indicated with solid lines; uncertain boundaries are denoted by question marks; unconformities are indicated by plus (++) symbols. Intervals without ages indicated are barren of diagnostic microfossils. Detailed information on biostratigraphic zonations and paleomagnetic stratigraphy appears in the "Biostratigraphy" and "Paleomagnetism" sections, respectively, of each site chapter report.

Sedimentary Structures

Primary biogenic and physical sedimentary structures are indicated by symbols entered in the "Structure" column of the core description forms. Figure 2 shows all of the symbols used during Leg 156. The structures observed include trace fossils (burrows and feeding trails), horizontal laminae, graded beds, ripple cross-laminae, and sediment rip-up clasts. In instances where the sedimentary structures were too detailed to be depicted on the barrel sheets (e.g., Cores 156-948C-17X through -19X), they were omitted and the reader is directed to view the core photos or VCDs for accurate information.

Sediment Disturbance

Sediment disturbance resulting from the coring process is illustrated in the "Disturbance" column on the core description forms (using symbols in Fig. 2). Blank regions indicate an absence of drilling disturbance. The intensity of drilling disturbance for soft sediments conforms to the following categories: (1) slightly deformed: bedding contacts are slightly bent; (2) moderately deformed: bedding contacts have undergone extreme bowing; (3) highly deformed: bedding is completely disturbed, in some cases, showing diapirlike or flow structures; (4) soupy: intervals are water saturated and have lost all aspects of original bedding.

The degree of fracturing in more indurated sediments falls into one of the following four categories: (1) slightly fractured: core pieces are in place and contain little drilling slurry or breccia; (2) moderately fragmented: core pieces are in place or partly displaced, but original orientation is preserved or recognizable (drilling slurry surrounds drilling "biscuits"); (3) highly fragmented: pieces are from the interval cored and probably in correct stratigraphic sequence (although they may not represent the entire section), but original orientation is completely lost; (4) drilling breccia: core pieces have

lost their original orientation and stratigraphic position and may be mixed with drilling slurry.

Samples

The positions of discrete samples for shipboard analysis and whole-round samples are indicated in the "Samples" column on the VCDs. The symbols used in this column are as follows:

- I = interstitial water whole-round sample,
- W = all other whole-round samples,
- P = physical properties sample,
- S = smear slide sample,
- T = thin-section sample,
- M = paleontology sample, and
- X = paleomagnetic sample.

In most instances, physical properties samples also were analyzed for carbonate content and bulk X-ray mineralogy. Actual centimeter-intervals from which whole-round samples were taken are included at the bottom of the "Description" column; these centimeter-intervals may vary slightly from those shown in the core photographs, as a result of movement of core in the liner during splitting.

Color

Redox-associated color changes typically occur when deep-sea sediments are exposed to the atmosphere. Because of changes in color, hue, and chroma, attributes were determined as soon as possible after the cores were split, using a Minolta CM-2002 hand-held spectrophotometer. The color scanner measures reflected visible light in 31 10-nm-wide bands that range from 400 to 700 nm. Reflectance measurements were taken at 5-cm intervals on all cores. Average core colors, rounded off to the closest standard Munsell notations, appear in the "Color" column on the core description form. In some cores (e.g., Cores 156-948C-13X through -19X), color changes are on too fine a scale to be depicted in the "Color" column; in these instances, color information appears in the "Description" column.

Written Description

The written description for each core consists of five parts: (1) a heading that lists the major sediment lithologies; (2) a brief description of the major lithologies; (3) a brief description of the minor lithologies (if any); (4) a brief description of the structural features (if any); and (5) specific locations of whole-round samples taken for shore-based analyses.

Structural Geology

Three types of structural geology deformational features are included on the "barrel sheets": (1) bedding dip; (2) intervals of scaly fabric; and (3) occurrences of various other deformation features. These features are shown in three separate columns, on the left side of the "barrel sheets." Symbols used in these columns are illustrated in Figure 2.

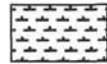
Smear Slide Summary

A table summarizing data from smear slides and thin sections appears at the end of each site chapter. The table includes information on the sample location, whether the sample represents a dominant ("D") or a minor ("M") lithology in the core, and the estimated percentages of sand, silt, and clay, together with all identified components. We emphasize here that smear slide analyses provide crude estimates of the relative abundances of detrital constituents; the mineralogies of finer-grained particles are difficult to identify petrographically, and sand-sized grains tend to be underestimated because they cannot be incorporated into the smear evenly. In addition, esti-

Biogenic pelagic sediments

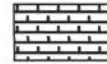
Calcareous

Nannofossil ooze



CB1

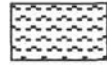
Nannofossil chalk



CB5

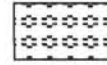
Siliceous

Radiolarian ooze



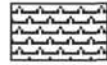
SB2

Siliceous ooze



SB3

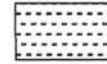
Radiolarite



SB5

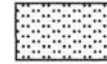
Siliciclastic sediments

Clay/claystone



T1

Silt/siltstone



T5

Silty sand/sandy silt



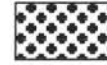
T7

Silty clay/clayey silt



T8

Gravel



SR1

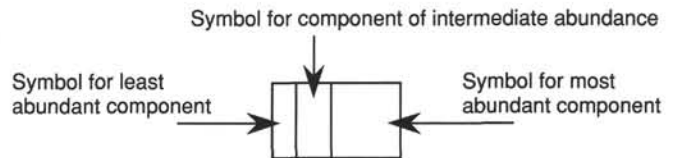


Figure 1. Key to symbols used in the "Graphic Lithology" column on the core description forms ("barrel sheets").

mates of grain size suffer from systematic errors because of differences between the surface areas of grains and their respective weight percentages; this is particularly problematic with clay-sized particles and nannofossils.

Sediment Classification

Leg 156 used the sediment classification scheme of the Ocean Drilling Program (Mazzullo et al., 1988) for granular sediment types. Four grain types occur in granular sediments: pelagic, neritic, siliciclastic, and volcanoclastic. Pelagic grains are fine-grained skeletal debris produced by open-marine siliceous and calcareous microfauna and microflora (e.g., radiolarians, coccoliths, discoasters, foraminifers). Neritic grains are coarse-grained calcareous skeletal fragments (e.g., bioclasts, peloids) and fine-grained calcareous grains of non-pelagic origin. These types of grains were not encountered during Leg 156. Siliciclastic grains comprise minerals and rock fragments that were eroded from plutonic, sedimentary, and metamorphic rocks. Volcanoclastic grains include glass shards, rock fragments, and mineral crystals that were produced by volcanic processes.

Variations in the relative proportions of these four grain types define five major classes of granular sediments: (1) pelagic; (2) neritic; (3) siliciclastic; (4) volcanoclastic; and (5) mixed sediments (Fig. 3). Pelagic sediments contain >60% pelagic plus neritic grains, <40% siliciclastic plus volcanoclastic grains, and a higher proportion of pelagic than neritic grains. Neritic sediments include >60% pelagic plus neritic grains, <40% siliciclastic plus volcanoclastic grains, and a higher proportion of neritic than pelagic grains. Siliciclastic sediments are composed of >60% siliciclastic plus volcanoclastic grains, <40% pelagic plus neritic grains, and a higher proportion of siliciclastic than volcanoclastic grains. Volcanoclastic sediments contain >60% siliciclastic plus volcanoclastic grains, <40% pelagic and neritic grains, and a higher proportion of volcanoclastic than siliciclastic grains. The volcanoclastic category includes epiclastic sediments (eroded from volcanic rocks by wind, water, or ice), pyroclastic sediments (products of explosive mag-

Drilling disturbance symbols

Soft sediments	
	Slightly disturbed
	Moderately disturbed
	Highly disturbed
	Soupy
Hard sediments	
	Slightly fractured
	Moderately fractured
	Highly fragmented
	Drilling breccia

Sedimentary structures

	Fining-upward sequence
	Horizontal laminae
	Cross laminae
	Sharp contact
	Gradational contact
	Graded bedding (normal)
	Ash layer
	Veins
	Macrofault
	Isolated mud clasts
	Pyrite nodule/concretion
	Scoured contact with graded bed

Structural geology deformation structures

	Phillipsite vein
	Rhodochrosite vein
	Sediment-filled vein
	Microfault (normal)
	Microfault (thrust)
	Macrofault (sense not determinable)
	Stratal disruption
	Core-scale fold
	Fracture network
	Brecciated zone

Figure 2. Symbols used for drilling disturbance, sedimentary structures, and deformation structures on core description forms (“barrel sheets”).

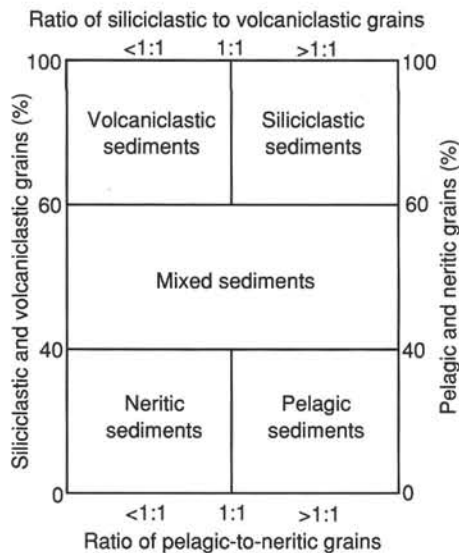


Figure 3. Classes of granular sediment (from Mazzullo et al., 1988).

ma degassing), and hydroclastic sediments (granulation of volcanic glass by steam explosions). Mixed sediments are composed of 40% to 60% siliciclastic plus volcanoclastic grains and 40% to 60% pelagic plus neritic grains.

All granular sediments are classified by designating a principal name plus major and minor modifiers. The principal name of a granular sediment defines its granular-sediment class; the major and minor modifiers describe the texture, composition, fabric, and/or roundness of the grains themselves (Table 1). Only sediment types encountered during Leg 156 are discussed below.

Principal Names

Each granular-sediment class has a unique set of principal names. For pelagic sediment, the principal name describes the composition and degree of consolidation using the following terms: ooze = unconsolidated calcareous and/or siliceous pelagic sediment; chalk = firm pelagic sediment composed predominantly of calcareous pelagic grains. Texture provides the main criterion for selecting a principal name for siliciclastic sediment. The Udden-Wentworth grain-size scale (Fig. 4) defines the grain-size ranges and the names of the textural groups (sand, silt, clay) and subgroups (fine sand, coarse silt, etc.). Where two or more textural groups or subgroups are present, the principal names appear in order of increasing abundance (e.g., silty clay). Ten major textural categories can be defined on the basis of relative proportions of sand, silt, and clay (Fig. 5). In practice, distinctions between some of the grain-size categories are dubious without accurate measurements of weight percentages. It is especially difficult to recognize relative proportions of fine silt and clay; thus, a rigorous boundary was not placed between silty clay and clayey silt. For lithified sediments, the suffix “-stone” is affixed to the principal names sand, silt, and clay. Only fine-grained volcanoclastic material (less than 2 mm in diameter) was encountered during Leg 156. The name “volcanic ash” applies to unlithified pyroclasts; for lithified material, the term “tuff” is used. With mixed sediment, the principal name describes the degree of consolidation. The term “mixed sediment” is used for unlithified sediment, and the term “mixed sedimentary rock” is used for lithified sediment.

Major and Minor Modifiers

To describe the lithology of the granular sediment in greater detail, the principal name of each granular-sediment class can be preceded by major modifiers and followed by minor modifiers (Table 1). Minor modifiers are preceded by the term “with.” The most common uses of major and minor modifiers are to describe the composition and tex-

Millimeters	μm	Phi (ϕ)	Wentworth size class
4096		-20	Boulder (-8 to -12 ϕ)
1024		-12	
256		-10	
64		-8	Cobble (-6 to -8 ϕ)
16		-6	
4		-4	Pebble (-2 to -6 ϕ)
3.36		-2	
2.83		-1.75	Granule
2.38		-1.50	
2.00		-1.25	
1.68		-1.00	
1.41		-0.75	
1.19		-0.50	Very coarse sand
1.00		-0.25	
0.84		0.00	Coarse sand
0.71		0.25	
0.59		0.50	
1/2 — 0.50	500	0.75	
0.42	420	1.00	
0.35	350	1.25	Medium sand
0.30	300	1.50	
1/4 — 0.25	250	1.75	
0.210	210	2.00	Fine sand
0.177	177	2.25	
0.149	149	2.50	
1/8 — 0.125	125	2.75	
0.105	105	3.00	Very fine sand
0.088	88	3.25	
0.074	74	3.50	
1/16 — 0.0625	63	3.75	Coarse silt
0.0530	53	4.00	
0.0440	44	4.25	
0.0370	37	4.50	
1/32 — 0.0310	31	4.75	Medium silt
1/64 0.0156	15.6	5	
1/128 0.0078	7.8	6	Fine silt
1/256 — 0.0039	3.9	7	
0.0020	2.0	8	Very fine silt
0.00098	0.98	9	
0.00049	0.49	10	Clay
0.00024	0.24	11	
0.00012	0.12	12	
0.00006	0.06	13	
		14	

Figure 4. Udden-Wentworth grain-size scale (in millimeters) for siliciclastic sediments, together with comparable values in ϕ units and standard sieve mesh sizes (from Pettijohn et al., 1973).

ture of grain types that are present in major (greater than 25%) and minor (10%–25%) proportions. In addition, major modifiers can be used to describe grain fabric, grain shape, and sediment color. The nomenclature for major and minor modifiers is as follows:

1. The composition of pelagic grains can be described in greater detail with major and minor modifiers, such as diatomaceous, radiolarian, nannofossil, and foraminiferal. The terms siliceous and calcareous are used to describe sediments that are composed of siliceous or calcareous pelagic grains of uncertain origin.

2. The textural designations for siliciclastic grains utilize standard major and minor modifiers, such as sandy, silty, and clayey. The character of siliciclastic grains can be described further by mineralogy, using modifiers such as quartzose, feldspathic, smectitic, zeolitic, lithic, or calcareous.

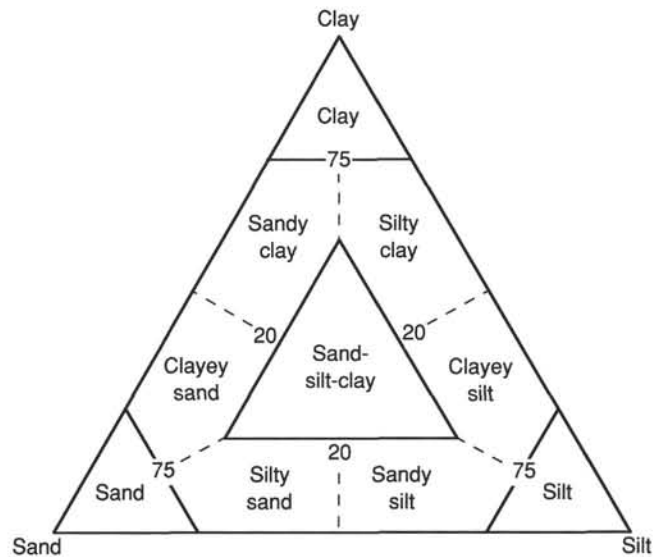


Figure 5. Ternary classification scheme for siliciclastic sediment textures (modified from Shepard, 1954).

3. Major and minor modifiers help define compositional details of volcanoclastic grains. Common terms include “lithic” (rock fragments), “vitric” (glass shards and pumice), and “crystal” (fresh euhedral mineral crystals). Modifiers also describe the compositions of the lithic grains (e.g., basaltic) and crystals (e.g., feldspathic).

X-Ray Diffraction

The mineralogy and relative abundances of common minerals were analyzed on bulk samples using standard X-ray diffraction techniques. Bulk samples were oven-dried or freeze-dried, ground to a fine powder with a ball mill, then packed into rectangular aluminum holders. The randomly oriented powders were not pre-treated with any chemicals.

The X-ray laboratory aboard the *JOIDES Resolution* is equipped with a Phillips PW-1729 X-ray generator, a Phillips PW-1710/00 diffraction control unit with a PW-1775 35-port automatic sample changer, and a Phillips PM-8151 digital plotter. Machine settings used were as follows: generator = 40 kV and 35 mA; tube anode = Cu; wavelength = 1.54056 Å (CuK α_1) and 1.54439 Å (CuK α_2); intensity ratio = 0.5; focus = fine; irradiated length = 12 mm; divergence slit = automatic; receiving slit = 0.2 mm; step size = 0.005°2 θ ; count time per step = 1 s; scanning rate = 2°2 θ /min; ratemeter time constant = 0.2 s; spinner = off; monochromator = on; scan = continuous; scanning range = 2°2 θ –35°2 θ .

Digital data were processed using a Phillips peak-fitting program that subtracts background intensities and fits ideal curve shapes to individual peaks or ranges of peaks, as specified by the operator. Typically, this program was used over the following scanning angles: 3.5°–10.5°2 θ (smectite and illite), 10.5°–13.5°2 θ (kaolinite + chlorite) and 25.5°–30.5°2 θ (quartz, plagioclase, and calcite). Curve-fitting is most effective if the steps per scanning interval are less than 750, and iterations continue automatically until a prescribed χ -square test is satisfied. Output of the processed digital data includes the angular position of each peak (°2 θ), d -spacing (Å), peak width (Δ °2 θ), intensity or height (counts per second above background), and peak area (total counts above background). Graphics output produces continuous tracings of the diffraction peaks with intensity units of counts per second.

In addition to the routine identification of important detrital and diagenetic minerals, we estimated relative abundances of the dominant minerals. Correction factors for integrated peak areas were calculated by matrix inversion using data from mineral calibration standards (Fisher and Underwood, this volume). Mineral abundances

Table 1. Outline of the ODP classification scheme for granular sediment (modified from Mazzullo et al., 1988).

Sediment class	Major modifiers	Principal name	Minor modifiers
Pelagic sediment	Composition of pelagic and neritic grains present in major amounts Texture of clastic grains present in major amounts	Chalk Limestone Radiolarite Diatomite Spiculite Chert	Composition of pelagic and neritic grains present in minor amounts Texture of clastic grains present in minor amounts
Neritic sediment	Composition of neritic and pelagic grains present in major amounts Texture of clastic grains present in major amounts	Boundstone Grainstone Packstone Wackestone Mudstone Floatstone Mudstone	Composition of neritic and pelagic grains present in minor amounts Texture of clastic grains present in minor amounts
Siliciclastic sediment	Composition of all grains present in major amounts Grain fabric (gravels only) Sediment color (optional) Grain shape (optional)	Gravel Sand Silt Clay	Composition of all grains present in minor amounts. Texture and composition of siliciclastic grains present as matrix (for coarse-grained clastic sediments)
Volcaniclastic sediments	Composition of all volcaniclasts present in major amounts Composition of all pelagic and neritic grains present in major amounts Texture of siliciclastic grain present in major amounts	Breccia Lapilli Ash/tuff	Composition of all volcaniclasts present in minor amounts Composition of all pelagic and neritic grains present in minor amounts Texture of siliciclastic grains present in minor amounts
Mixed sediments	Composition of neritic and pelagic grains present in major amounts Texture of clastic grains present in major amounts	Mixed sediments	Composition of neritic and pelagic grains present in minor amounts Texture of clastic grains present in minor amounts

Table 2. Common minerals analyzed by X-ray diffraction, with associated peak positions.

Mineral	Window ($^{\circ}2\theta$, $\text{CuK}\alpha_1$)	d -spacing (\AA)
Calcite	29.25–29.60	3.05–3.01
Kaolinite + chlorite	12.39–12.60	7.14–7.02
Illite	8.75–9.10	10.10–9.72
Plagioclase	27.80–28.15	3.21–3.17
Quartz	26.65	3.34
Smectite	5.73–6.31	15.42–14.01

have been normalized to 100%. Diagnostic peak positions are shown in Table 2. Relative percentages of total clay minerals are based on the sum of the weighted areas of three individual clay-mineral peaks: smectite (001), illite (001), and [kaolinite (001) + chlorite (002)]. These methods differ from the one used during Leg 110 on the Barbados Ridge (Masle, Moore, et al., 1988), whereby the total clay-mineral content was calculated from a single composite peak at approximately $19.75^{\circ}2\theta$. Data from Leg 110, moreover, are based on peak intensities, rather than integrated areas; a set of calibration factors derived from mixtures of different mineral standards; and a Philips software package for quantitative analysis. Comparisons among these techniques and their associated errors are discussed in Fisher and Underwood (this volume).

Because of the presence of small quantities of crystalline minerals not included in our calculations, plus amorphous solids (volcanic glass, biogenic silica, organic matter, poorly formed clay crystallites, and so forth), the relative abundances reported here may be significantly greater than the true weight percentages. No attempt was made to quantify the weight percent of amorphous material; past studies in the west-central Atlantic region, however, have indicated amorphous contents as high as 40% to 70% (e.g., Fan and Rex, 1972), based on the amount of diffuse scatter in the total X-ray intensity (Cook et al., 1975).

Calculations of relative percentages of each mineral within the clay-mineral group suffer from potentially large errors when analyzed as untreated, air-dried, random powders. The diagnostic kaolinite (001) peak, for example, interferes with the chlorite (002) peak at approximately $12.5^{\circ}2\theta$; thus, the weighted intensity of this peak

should be regarded as an undifferentiated composite. Similarly, unless samples have been saturated with ethylene glycol to expand the smectite lattice to 17\AA , the (001) chlorite, (001) illite, and mixed-layer illite/smectite peaks overlap with discrete smectite at approximately 6° to $9^{\circ}2\theta$. Smectite content, therefore, may be slightly overestimated in samples that contain abundant discrete chlorite, illite, or illitic mixed-layer clay.

STRUCTURAL GEOLOGY

Introduction

Leg 156 was designed to improve understanding of the interaction between deformation and fluid processes in an accretionary prism, especially in the region of the décollement. Hence, the coring program focused on the décollement, and the prime task of the structural geologists was to extract all the relevant structural data from the material recovered from this zone. This information, besides documenting the mechanical and hydrogeological behavior of the décollement, helps to elucidate the configuration of the prism toe and provides a link between the stratigraphic, physical, geochemical, and other aspects of the prism that were studied during the cruise.

As the Ocean Drilling Program has progressed, the attention given to structural investigation of cores recovered from accretionary prisms has been gradually increasing, together with growing efforts to treat the information as quantitatively as possible. Parallel advances have been taking place during cruises that investigate other tectonic settings.

However, the ways in which the structural data have been handled and recorded have tended to differ somewhat from cruise to cruise, usually as a result of impromptu discussions on board the ship. In contrast to the long-established procedures for reporting most shipboard data, until now, there has been no ODP guidance about how the structural geological data should be treated. Inventing a custom-designed procedure for each cruise does offer flexibility and scientific advantages, but tends to lead to the data remaining unpublished and unconsulted by other workers.

Against this background, ODP policy at the time of writing, driven by recommendations from the Tectonics Panel (TECP), was to establish a standardized format for the recording and publishing of structural geological data. The structural geologists on Leg 156 were charged with testing and refining such a formalized system. Therefore, the explanation below, in addition to reporting how the structures were dealt with in the core, summarizes our attempts to establish a practicable, yet realistic, scheme for standardized recording of structural information from sedimentary materials.

Occurrence of Structures in the Cores

An unusually large number of whole-round core samples were taken during this leg, in line with the goals of measuring deformational and fluid-flow properties of the prism, but this still amounted to less than 10% of the total recovered material. We examined all the remaining core for structures down to the hand-lens scale. The work was based on the face of the archive half of the split core, although we made frequent recourse to the working half of the core for additional information and, especially, for orientation data. Much use was made of scalpels and glass slides to skim away gently the film of mud smeared during the splitting of the core.

Reports from previous cruises have noted the difficulty of distinguishing natural structures from the results of disturbance because of core-splitting, stress release, desiccation, and fluid expansion. Especially frustrating during this cruise was the propensity of the cores to develop drilling biscuits and a range of related structures, which can both mimic and pass into natural equivalents. For example, some foliations, apparently well preserved within otherwise intact biscuits, and hence thought to be natural, have equivalents developed in the drilling debris that surrounds the biscuits; some fractures were judged to have involved drilling disturbance, but might well have evolved from pre-existing natural structures. Although noting the recommendations of Lundberg and Moore (1986, p. 42–43), in the cores described here, we found that diagnosing natural structures was a formidable problem. We decided to adopt a conservative approach and to report only those features that we judged to be largely of natural origin. We, therefore, have confidence in the structures discussed here, but it may be that the magnitude of natural deformation in the cores has been under-reported, particularly for weak effects.

The occurrence of each feature in the core was recorded on a "Structural Description Sheet" (Fig. 6). Its design is based on that first used during Leg 131 and progressively refined during subsequent cruises, in particular, Legs 134, 141, 146, 147, and 149. The location of an item of interest was recorded as the distance in centimeters of the top and the bottom of the structure from the top of the section. Features such as a horizontal bedding plane, therefore, would have two identical depth values, whereas a thicker structure, such as a zone of scaly fabric, would have differing values and could occupy a considerable interval of the core and section. The depth of occurrence below the seafloor (mbsf) was added later for selected structures as that information became available for each core. Observers during earlier cruises found it useful to assign a number to each separate piece of core, for example, in case the piece should be removed for analysis elsewhere, and to each individual structure, for purposes of cross-referencing. Columns on the sheet are available for these procedures, although we found them unnecessary.

Description of Structures Seen in the Cores

An important aspect of the structural database was the construction of a list of those terms most useful for describing deformational structures seen in ODP cores (Table 3). Following advice from ODP headquarters, we avoided a separate scheme for sedimentary rocks, as opposed to igneous and sedimentary rocks, which was seen as counter to the goals of the standardization, because many of the structures are common to both groups of materials. However, our deliberations during this cruise were confined to features of sedimentary rocks, and hence the accompanying short definitions of terms (Table 4) have been confined to those structures. We have not attempted to modify the terms that were suggested to us for igneous and metamorphic rocks; the optimum ways of dealing with these will emerge from cruises concerned with those materials.

Before constructing the list, we reviewed the structural information in relevant *Initial Reports* volumes and in the compilation of Lundberg and Moore (1986). We deliberately attempted to keep the list short, and, indeed, our review indicated that only a relatively small number of structures have been commonly recorded during shipboard investigations. Most of the terms defined by Lundberg and Moore (1986) continue to be widely used, although spaced foliation and kink band have been subsumed by deformation band, and crenulation foliation has not been widely identified. Vein structure is now more often referred to as sediment-filled veins. Scaly fabric is given two entries because of the need to record separately aspects of the fabric itself and of the overall zone, and other structures that occur in narrow zones may have to be treated in the same way. Note that for thick zones the top and bottom intervals may well specify the thickness adequately, but inclined narrow zones have a thickness that differs from the core intervals. The term fracture network emerged during the course of Leg 156 to be useful; its meaning and use are explained in detail in the "Structural Geology" section of the "Site 949" chapter (this volume).

The listed terms should allow names to be given to structures during routine shipboard core description (i.e., fairly quickly, reproducibly, and based on observations no more detailed than those possible with a hand lens). Some terms, of which a good example is deformation band, group a number of structures that are not all of related origin, but which can be clearly distinguished only by detailed study (Maltman et al., 1993). In other cases, for example, scaly fabric, the origin and kinematic significance of the structure, which also may be polygenetic, is a matter of uncertainty. However, we consider that introducing a new or different term, or deferring the naming of the structure until detailed laboratory study is completed, is neither desirable nor practical. We are conscious of the pitfalls and shortcomings of such schemes as that proposed here. However, its use should mitigate some of the problems of consistency of usage—between individuals, teams on different shifts, and shipboard parties—as well as the division of gradational and overlapping structures into discrete types (e.g., Taira, Hill, Firth, et al., 1991; Behrmann, Lewis, Musgrave, et al., 1992).

A column on the description sheet allows the observer to note the intensity of development of a structure. Although the original suggestion of ODP involved a numerical scale from 1 to 5, during this cruise we found a scale of 1 to 3 to be more practical (equivalent to incipient, moderate, and intense development), and even then only found it useful for scaly fabrics.

The comments column of the description sheet allowed descriptive details to be recorded, and while most of these are not meant for publication, many were utilized later in the site descriptions and in structural interpretations. The comments column of the description sheets was used to record information beyond that specified in the other columns, for example, the magnitudes of fault separation, style of folding, and comments on the quality of measurements.

In an attempt to balance the terminological crudeness of our database scheme, care was taken to sketch many of the features and to ensure that the sketches were properly archived. A "Sketch Summary

Structural description sheet

Leg 156 Site 948 Hole C Core 5x Observers AM, PL Summary comments *Gray claystone, highly bioturbated, 2-4 cm drilling biscuits*

section	depth (cm)		depth mbsf	piece #	feature #	feature identifier	intensity if approp.	depth of measurmnt	core face orientation		2nd appt. orientation		core reference frame		Comments
	top	base							appt. dip	direction	dip angle	direction	strike/trend	dip/plunge	
1	7	10				B			22	270	30	180	061	56	based on zoophycos
	49	50				CTV			36	090	35	235	072	67	gray-green to brown transition in mud, probably bedding
	54	66				B			42	270	-true	-	180	42	series of parallel zoophycos tubes:  [PMAG]
2															structureless drilling biscuits, bioturbated. reliable bedding not apparent
3															structureless drilling biscuits, much drilling slurry
4	74	74				B			horiz.	21	000	270	21	21	based on zoophycos tube [PMAG]
	82	84				B			13	270	20	000	238	23	"
	84	85				B			55	270	0	000	180	55	"
5	62	65				B			4	270	32	180	096	32	zoophycos: well developed [PMAG]
	67	68				B			21	090	03	000	352	21	"
	72	72				B			09	270	17	000	243	19	[PMAG]
	142	145				B			45	270	16	180	164	46	"
	148	149				B			06	270	05	000	220	08	[PMAG]
6	17	18				B			26	270	0	000	180	26	heavily bioturbated: bedding indicated only by [PMAG]
	112	112				B			20	270	09	000	204	22	zoophycos tubes [PMAG]
7															much broken by drilling: 2cm biscuits only 3/3 width of core. bioturbated and structureless
CC															less biscuitized than section 7, but structureless

Figure 6. Example of a structural description sheet used during core description.

Table 3. List of terms used for identifying structural features in cores.

Structural feature	Identifier abbreviation	Data recorded
Bedding	B	Strike/dip of bedding surface
Color/texture variation	CTV	Strike/dip of separating surface
Fissility	Fiss	Strike/dip of parting surface
Joint	J	Strike/dip of joint surface
Mineral vein	V	Strike/dip of margin; plunge/trend of fibers
Magmatic vein	MV	Strike/dip of vein margin
Sediment-filled vein	SV	Strike/dip of vein/array boundary
Fault	F	Strike/dip of fault surface
Fault, normal	Fn	Strike/dip of fault surface
Fault, reverse	Fr	Strike/dip of fault surface
Fault, strike-slip	Fss	Strike/dip of fault surface
Fault, oblique-slip	Fob	Strike/dip of fault surface
Breccia zone	BZ	Strike/dip of zone boundary; zone thickness
Deformation band	DB	Strike/dip of band boundary; band thickness
Stylolite	St	Strike/dip of surface; plunge/trend of peaks
Stratal disruption	SD	Strike/dip of overall bedding, where appropriate
Scaly fabric	SF	Strike/dip of foliation
Scaly fabric zone	SFZ	Thickness of zone; strike/dip of zone margin
Spaced foliation	SpFol	Strike/dip of foliation
Fold	FO	Axial surface strike/dip; hinge line trend/plunge
Slickenline	Sl	Plunge and trend of slickenline surface
Other linear structure	L	Plunge and trend
Magmatic fabric	M	Strike/dip or plunge/trend
Mineral shape fabric	MSF	Strike/dip or plunge/trend
Ductile shear zone	DSZ	Strike/dip of zone margin
Magmatic contacts	MC	Strike/dip of contact surface
Other planar structure	P	Strike/dip

Table 4. Short, working definitions of terms used to describe structures in sedimentary rock cores.

Structure feature	Term
Bedding	Primary depositional layering, generally taken to mark horizontal at the time of initial sedimentation.
Breccia zone	Zone of angular rock fragments, commonly set in a matrix that may be composed of similar material, finely comminuted rock ("fault gouge"), or secondary minerals.
Color/texture variation	A change in the color and/or the texture of sedimentary material not clearly related to an identifiable structural feature. Some changes may reflect bedding.
Deformation band	Narrow (less than a centimeter wide), essentially planar zone of displacement, but excluding clear faults. Includes kinklike, shear zonelike and faultlike varieties. Commonly appears dark in fresh core, and may merely deflect bedding or fissility.
Fault	Fracture along which slip has occurred as indicated by displacement of an earlier feature across the fracture or the presence of slickenlines. In cores, faults range from discrete sharp fractures to broad fracture zones.
Fissility	Closely spaced parting surfaces developed in fine-grained rocks, parallel to bedding. Commonly increases in intensity downhole and is normally absent from strongly bioturbated rocks. Commonly interpreted as a product of compaction.
Fold	A curve or bend imposed on a rock structure. Includes both discrete folds and disharmonically contorted layers that may be of nontectonic origin.
Joint	Discrete fracture on which there has been no displacement parallel to the surface of the fracture.
Mineral vein	A vein occupied by a mineral or mineral aggregate that differs from nearby material in terms of composition and/or texture and that has crystallized or recrystallized in situ.
Scaly fabric	Closely spaced, variably anastomosing commonly slickensided surfaces. Shows a range in intensity, with more weakly developed varieties delineating fragments that are several millimeters wide and of low aspect ratio. With increasing intensity, fragments decrease in size and their aspect ratio increases, so that where most intense, the structure is almost planar (scaly foliation of Lundberg and Moore [1986]).
Sediment-filled vein	Planar or sigmoidal vein filled by normally fine-grained sediment. Usually part of an array oriented nearly perpendicular to the orientation of the individual vein. Found mostly in mudstone or claystone.
Slickenline	Lineation occurring on a slickenside. May be a product of mineral fiber growth, abrasion, the streaking out of comminuted rock particles, and so forth.
Slickenside	Smoothed or polished surface, presumably indicating movement. Particularly associated with faults, scaly fabric, and some deformation bands.
Stratal disruption	Discontinuous bedding attributed to, or enhanced by, deformation. Inferred processes include boudinage, closely spaced faulting, and offset along crosscutting foliations. May be difficult to demonstrate lithological layering is unequivocally bedding, not, for example, deformed bioturbation.
Stylolite	Wavy or jagged seams most commonly encountered in chalk and limestone and in which the seams are occupied by clay. Seams range from narrow films to braided structures up to a centimeter wide. Widely accepted as a product of pressure solution.
Other planar structures	Planar structure of uncertain character or not defined above.
Other linear structure	Elongate feature, including oxidation/reduction spots, bioturbation structures, intersection lineations, and linear structures of uncertain character or not defined above.

Sheet" was used expressly for this purpose; examples appear in the site chapter reports that follow in this volume. All sketches were executed in permanent black ink. In addition to recording the appearance of structures more precisely than can be done with words, such a sheet provides a useful graphical summary of each section. For smaller but important structures, the correct scaling was attained by tracing the structures onto acetate sheets and then transferring the tracing onto the form.

Orientation of Structures Within the Cores

A primary task of shipboard structural geologists is to record the orientations of structures seen in the cores, and for this we made much use of the protractor device described in Taira, Hill, Firth, et al. (1991, p. 42). However, relating these measured orientations to their real subsurface disposition has long been a problem, and we approached it in the same way as was employed during recent cruises. Briefly, two steps are required. First, the orientation of a structure *within the core reference frame* has to be calculated, normally from the apparent dip in the core face and in another known direction. Second, the orientation of the core has to be related to *geographic north*, and the orientation of the structures adjusted accordingly. Details are described in Westbrook, Carson, Musgrave, et al. (1994) for sediments and sedimentary rocks and in Gillis, Mével, Allan, et al. (1993) for igneous and metamorphic rocks.

In general, the first stage can be done routinely, although if structures are abundant, it does require collecting and converting a large number of apparent measurements. The dips of structures measured in the split core were written on the description sheet, following the convention shown in Figure 7. That is, apparent dips were expressed as two-digit angles between 00° and 90°, together with the dip directions as three-digit azimuths that originated orthogonally within the archive half at 000°. Core-face dip directions thus would be either 090° or 270°. Dip directions were preferred over strike to be consistent with the correction software.

Where a structure was seen as a three-dimensional plane in a fragmented piece of core, or its trace could be observed at the top or bottom of a core section, it was possible to measure the true orientation directly in the core reference frame. In the studied cores, the second apparent dip angle and direction were most commonly obtained from the corresponding part of the working half of the core, as explained in Figure 7. Note that dips recorded assume that the long axis of the core is vertical; that is, deviations of the drill hole from vertical have been ignored.

Linear features were measured using the technique outlined in Westbrook, Carson, Musgrave, et al. (1994; see especially figs. 6A and 6B), but few such structures were encountered during this cruise. Surfaces associated with the scaly fabric are commonly lineated, and we began measuring these in the hope of conducting stress-tensor analysis. However, we abandoned this endeavor after realizing that almost every surface within the cores, including those that appeared to have been induced by drilling, had been lineated to some extent. It seems that surfaces within the clayey lithologies encountered here have a particular propensity for taking on a lineated aspect, and we viewed it as impossible to isolate slickenlines that were of unequivocal natural origin.

After completing a session of core description, we entered the orientation data into a "Structural Data Sheet," of the kind illustrated in Figure 8. Being a spreadsheet (here operating in Microsoft Excel), this form provides for easy storage, retrieval, and manipulation of these data. However, we found it convenient to calculate the true orientations using the Stereonet plotting program of R. W. Allmendinger, version 4.25a, as detailed in Westbrook, Carson, Musgrave, et al. (1994), for entry into the spreadsheet. Many of the headings for the various columns are tersely abbreviated, so that they occupy the single row required by Microsoft Excel version 4. The columns showing site, hole, and core type may seem superfluous, but are required to

employ the ODP macro for converting interval depths in the section to depths below the seafloor.

The most important aspects of all these data have been abstracted and summarized on the "barrel sheet" for each core (see "Lithostratigraphy and Sedimentology" section, this chapter). These "barrel sheets" have been reproduced at the end of each site chapter.

Geographic Orientation of the Structures

Following the derivation of orientation data within the cores as outlined above, one must convert these local orientations to geographical coordinates. This stage depends on the availability of multishot, Formation MicroScanner (FMS), or paleomagnetic data. During Leg 156, only the last technique was possible. Because the cores almost ubiquitously had been broken into drilling biscuits, the procedure involved carefully extracting individual pieces from the cores and passing them through the cryogenic magnetometer (see "Paleomagnetism" section, this chapter). With the aid of the shipboard paleomagnetic specialist, we were able to interpret the orientation of the natural remanent magnetism in many of the drilling biscuits for which we had structural information. The steps for using the declination in the geographic correction are summarized in Table 5.

BIOSTRATIGRAPHY

Calcareous Nannofossils

Zonation

The nannofossil zonation used here is a modification of those proposed by Bukry (1973, 1975), Okada and Bukry (1980), and Gartner (1977). For the pre-Pleistocene assemblages, the low-latitude zonation of Bukry (1973, 1975) and code number of Okada and Bukry (1980) are referred to for the reader's convenience. For the Pleistocene, the zonation proposed by Gartner (1977) has been used as it provides better resolution. Zonal modifications adopted here are those proposed by Bergen (1984) and Clark (1990). Primary and secondary biostratigraphic-event zonal markers for the Cenozoic are shown in Figure 9.

Methods

Calcareous nannofossil assemblages were described primarily from the results of smear-slide observations of each core-catcher sample. Additional samples were studied as time permitted on board the ship. Slides were examined exclusively with a light microscope. In all cases, a magnification of 1250× was used in estimating abundances.

The following scale was used to specify the abundances of individual species:

- V (very abundant) = 100 specimens/field of view,
- A (abundant) = 10–100 specimens/field of view,
- C (common) = 1–10 specimens/field of view,
- F (few) = 1 specimen/1–10 fields of view,
- R (rare) = 1 specimen/10–100 fields of view, and
- P (present) = a few specimens per slide.

Occurrences of reworked species are indicated by lowercase letters. Specification of percentages of calcareous nannofossils present in each sample were as follows:

- A (abundant) = >50%,
- C (common) = between 10% and 50%,
- F (few) = between 1% and 10%,
- R (rare) = <1%, and
- B (barren) = none.

The assessment of preservation of calcareous nannofossils was based on the following criteria:

G (good) = There is little or no evidence of dissolution and/or overgrowth, diagnostic characteristics are preserved, and almost all specimens (about 95%) can be identified.

M (moderate) = Dissolution and/or overgrowth are evident, the number of delicate forms is reduced, and these are frequently broken.

P (poor) = Severe dissolution, fragmentation, and/or overgrowth has occurred, primary features may have been destroyed, and many specimens cannot be identified at the species level.

Planktonic Foraminifers

Zonation

For the zonation of planktonic foraminifers, the scheme of Bolli and Saunders (1985) was used.

Sampling Procedure and Preparation

Foraminiferal samples were taken from the core catcher. Additional samples from each section of core that contained planktonic foraminifers were processed to refine the zonation.

The sediments were disaggregated in a 10% solution of hydrogen peroxide and washed with a coarse (420 μm) and a fine (44 μm) sieve. After decantation, the residues were dried, sieved, and kept in small glass vials. Three grain-size fractions were sieved:

1. Very coarse fraction, >420 μm .
2. Coarse fraction, 250 to 420 μm .
3. Middle fraction, 63 to 250 μm .
4. Fine fraction, <63 μm .

The foraminifers were collected in "Franke" microfossil trays: first, a general tray that contained all the different foraminifers found in the residue was examined, then, individual morphotypes were selected and mounted on black (exposed) photographic (resin) paper in specially prepared trays.

Abundance and Preservation

Foraminiferal abundances were classified as follows:

A (abundant) = more than 40% of the association of foraminifers,
 F (frequent) = between 20% and 40% of the association,
 C (common) = between 5% and 20% of the association,
 R (rare) = present with less than 5% of the association, and
 B (barren) = absent.

Three grades of preservation of the foraminifers were recognized:

G (good) = well-preserved tests,
 M (moderate) = moderately preserved foraminifers, partly broken or partly affected by dissolution, and
 P (poor) = preservation is bad, mostly broken or almost dissolved skeletons.

Radiolarians

Zonation

The low-latitude zonation of Nigrini (1971) was used for identifying the ages of Quaternary radiolarians. Neogene and Paleogene radiolarian biostratigraphy is based on the zonations of Riedel and Sanfilippo (1978) and Sanfilippo et al. (1985), using the shipboard compilation of Cenozoic radiolarian biostratigraphy for low and middle latitudes of C. Nigrini and A. Sanfilippo (unpubl. data).

Sampling Procedure and Preparation

Most biostratigraphic data were obtained from the core-catcher samples. Based on continuous core observation and analysis of numer-

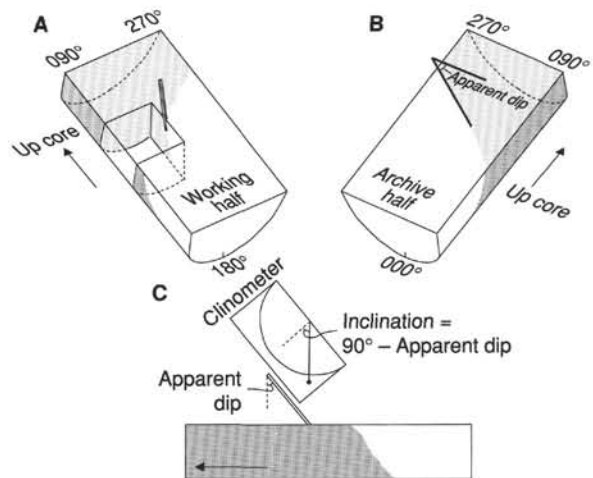


Figure 7. Diagram showing the conventions used for measuring azimuths and dips of structural features in cores. The core reference frame conventions for the working and the archive halves of the core can be seen in (A) and (B). The apparent dip of a feature in the face of the split core was measured first, generally on the face of the archive half (B). The data were recorded as an apparent dip toward either 090° or 270°. In the example shown, the apparent dip is toward 090°. A second apparent dip was measured by making a cut parallel to the core axis, but perpendicular to the core face, in the working half of the core (A) (most cuts were considerably smaller than the one represented in the diagram). The feature is identified on the new surface, and the apparent dip in the north-south direction (core reference frame) marked with a toothpick. The apparent dip is measured with a modified protractor (C) and quoted as a value toward either 000° or 180°. In this case, the apparent dip is toward 180° (into the working half). True dip and strike of the surface in the core reference frame then can be calculated from the two apparent measurements.

ous smear slides, intervals of radiolarian occurrences were located and sampled further.

The samples were dried and treated with 10% hydrogen peroxide, washed, and sieved. After subsequent drying, the material was sieved again. Grain-size intervals used were as follows:

1. Very coarse fraction, >250 μm .
2. Coarse fraction, between 250 and 150 μm .
3. Medium fraction, between 150 and 63 μm .
4. Fine fraction, <63 μm .

After final sieving, the radiolarians were randomly distributed on glass slides (strewn slides) and covered by a large cover slide after the radiolarian material was mounted, using an ultraviolet-light-activated mounting medium (Norland Optical Adhesive). One slide was made from each of the coarse and the fine fractions, and two slides from the medium fraction. In addition, radiolarian specimens were fixed in "Franke" microfossil trays on black resin paper for observation with reflected light.

Abundance and Preservation

The abundances of radiolarians were estimated from both glass slides and from the picking tray, because of sorting effects that can occur during shaking and spreading. Abundance ranges were described as follows:

- A (abundant) = more than 100 specimens per slide,
 C (common) = 10 to 100 specimens per slide,
 F (few) = 1 to 10 specimens per slide,
 R (rare) = present but rare or a trace, and
 B (barren) = absent.

Site	Hole	Core	Type	Sect.	Top	Bot.	Depth	#	ID	Thick.	Intens.	App. dip	App. trend	Strike	Dip	Reorient.	Geo. strike	Geo. dip	Comments
948	C	1	H	1	23	23	0.23		B					180	2				ash layer
948	C	1	H	1	31	32	0.31		B					270	12				ash layer
948	C	1	H	2	73	73	2.23		B					14	8				ash layer
948	C	1	H	2	92	92	2.42		B					180	2				ash layer
948	C	1	H	3	26	26	3.26		B					112	5				ash layer
948	C	1	H	5	123	124	7.23		B					121	6				ash layer
948	C	1	H	6	3	3	7.53		B					108	3				ash layer
948	C	2	X	1	93	99	421.73		B					45	21	paleomag.	351	21	aligned bioturbations
948	C	2	X	2	85	102	423.15		SFZ	7				231	13				upper boundary
948	C	2	X	2	86	88	423.16		V	0.05				208	20				rhodochrosite V parallel to SF, set
948	C	2	X	2	89	89	423.19		SF		3			19	45				upper limb of small FO
948	C	2	X	2	90	90	423.2		FO			6	90						FO hinge surface trace
948	C	2	X	2	91	91	423.21		SF		3			211	46				lower limb of small FO
948	C	2	X	2	91	91	423.21		FO					327	7				FO axial surface
948	C	2	X	2	96	99	423.26		SF		3			18	46				
948	C	2	X	2	99	102	423.29		SF		3			252	36				
948	C	2	X	3	23	39	424.03		SV	0.1				344	45				mud-filled, set
948	C	2	X	4	26	33	425.56		SFZ	7									low-angle
948	C	2	X	4	30	30	425.6		SF		2			311	55				
948	C	2	X	4	78	78	426.08		B					305	30				aligned coprolites
948	C	2	X	5	78	118	427.58		SFZ	40		37	270						upper boundary
948	C	2	X	5	77	80	427.57		V	0.05									rhodochrosite V parallel to SF, set
948	C	2	X	5	94	96	427.74		SF		3			13	47				
948	C	2	X	5	99	104	427.79		V	0.05				351	50				rhodochrosite V parallel to SF, set
948	C	2	X	5	111	111	427.91		B					343	51	paleomag.	320	51	<i>Zoophycos</i>
948	C	2	X	6	30	33	428.6		SV										mud-filled, set
948	C	2	X	CC	27	27	429.13		SV	0.1				183	32				mud-filled

Figure 8. Example of a structural data sheet, a spreadsheet used for the storage and manipulation of data derived from the core descriptions.

Table 5. A summary of the steps involved when converting measurements observed in split cores to real geographic coordinates.

Step	Summary of action
1	Identify features and measure apparent dips on archive half of core.
2	Look for auxiliary surfaces that provide further orientation information.
3	If necessary, refer to working half of core for auxiliary information. (Refer azimuths to 000 "pseudo-north" in the archive half.)
4	Derive true dip and azimuth orientation (e.g., using Stereonet Plotting Program of R.W. Allmendinger, plot apparent dip directions and angles as lines and find cylindrical best fit).
5	Correct dip angles for deviation of drillhole from vertical, if this information is available.
6	Select representative piece from continuously oriented part of core and pass through the cryogenic magnetometer. If the core section underwent little differential rotation during drilling, it may be reasonable to average the entire section. Derive the magnetic declination.
7	Adjust the magnetic declination by 180. (The paleomagnetic 000 reference point is located in the working half, 180 away from the reference point used in structural measurements). The adjustment is unnecessary if the magnetic declination of the working half was measured.
8	If the adjusted paleomagnetic declination falls between 000 and 180, subtract its value from the working azimuths to obtain the real strike, adjusting the dip direction as appropriate. If the adjusted paleomagnetic declination falls between 180 and 359, add its value to the working azimuths and adjust dip directions. These operations are conveniently performed stereographically (by rotating the orientations of the planes around a vertical axis by the required amount and in the appropriate direction), which allows both visual checking of the manipulation and direct printing of the results.

The preservation of tests was estimated using the following categories:

- G (good) = almost complete skeletons without recrystallization,
M (moderate) = partly broken specimens, tests partially recrystallized, or skeletons affected by dissolution, and
P (poor) = specimens mostly broken completely recrystallized.

Magnetostratigraphy

For comparison, Figure 9 shows a magnetic-polarity stratigraphic column based on the magnetic-polarity time scale of Cande and Kent (1992).

PALEOMAGNETISM

Laboratory Facilities

The paleomagnetic laboratory on board the JOIDES Resolution is equipped with two magnetometers: a pass-through cryogenic superconducting rock magnetometer manufactured by 2-G Enterprises (Model 760R) and a Molspin spinner magnetometer. For demagnetization of samples, the laboratory contains an alternating-field (AF) demagnetizer and a thermal demagnetizer (Models GSD-1 and TSD-1 by the Schonstedt Instrument Co.) that are capable of demagnetizing discrete specimens to 100 mT and 700°C, respectively. Partial anhysteretic remanent magnetization (pARM) can be imparted to discrete samples by a DTECH, Inc., PARM-2 system, which consists of two parallel coils mounted outside and on-axis with the AF-coil of the GSD-1 demagnetizer, and a control box. This device allows one to apply a bias field to a sample during AF demagnetization; the bias field can be switched on optionally only over a window of AF field intensity during the declining-field stage of the demagnetization cycle. In addition, an in-line AF demagnetizer, capable of 25 mT (2-G Model 2G600), is included on the pass-through cryogenic magnetometer track for demagnetization of continuous sections. All demagnetization devices and magnetometers are shielded within μ -metal cylinders.

The sensing coils in the cryogenic magnetometer measure the magnetic signal over about a 20-cm interval, and the coils for each axis have slightly different response curves. The widths of the sensing regions correspond to about 200 to 300 cm³ of cored material, all of which contributes to the signal at the sensors. The large volume of core material within the sensing region permits one to determine accurately the remanence for weakly magnetized samples, despite the

relatively high background noise related to the motion of the ship. The practical limit on the resolution of natural remanence of the core samples is often imposed by the magnetization of the core liner itself (about 0.1 mA/m = 10^{-7} emu/cm³).

The pass-through cryogenic magnetometer and its AF demagnetizer can be interfaced with an IBM PC-AT-compatible computer and are controlled by a BASIC program that has been modified from the original SUPERMAG program that was provided by 2-G Enterprises. The current versions (CUBE155 for discrete samples and MAG155 for split-core sections) of the SUPERMAG program were previously modified to compensate for end effects. To do so, the program multiplies the sensor output by the fraction of the total measured area that actually contains sediment. The spinner magnetometer used for measuring discrete samples was interfaced with a Macintosh SE-30 computer with a program brought on board the ship by D. Schneider (WHOI) for Leg 138.

Anisotropy of magnetic susceptibility (AMS) is measured on board the ship using a KLY-2 Kappabridge magnetic susceptibility bridge. The listed sensitivity of this device is about 1×10^{-8} (SI volume units). The magnetically noisy environment of the core laboratory reduces the sensitivity of the KLY-2 to about 1×10^{-6} (SI volume units).

The magnetic susceptibility of unsplit sections of core is measured with a Bartington Instruments Model MS1 susceptibility meter adapted with an MS1/CS 80-mm whole-core sensor loop set at 0.465 kHz. The area of core measured is determined by the full width of the impulse response peak at half maximum, which is less than 5 cm. The susceptibility sensor is mounted with the gamma-ray attenuation porosity evaluator (GRAPE) and *P*-wave logger on a multisensor track (MST). The susceptibility of discrete specimens can be measured on board the ship with the KLY-2 or with a sensor unit (type MS1B) attached to the Bartington susceptibility meter.

An Analytical Services Company (ASC) Model IM-10 impulse magnetizer also is available in the magnetics laboratory for studies of the acquisition of both stepwise and saturation isothermal remanence magnetization (IRM) by discrete samples. This unit can apply pulsed fields from 20 to 1200 mT.

Paleomagnetic Measurements

Pass-through Magnetometer

The bulk of the paleomagnetic measurements for Leg 156 were performed with the pass-through cryogenic magnetometer. Pass-through paleomagnetic values were routinely measured on the archive

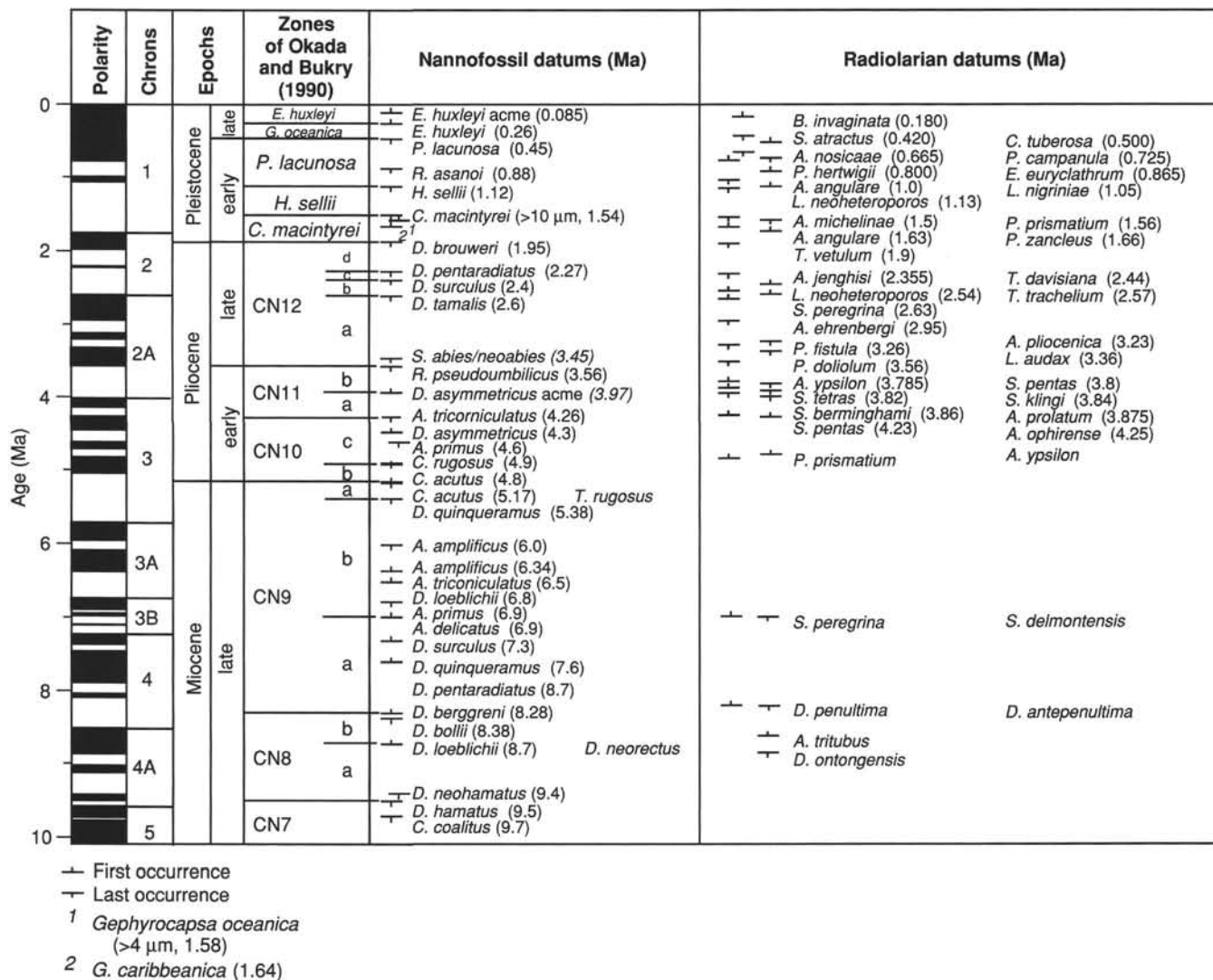


Figure 9. Cenozoic primary and secondary biostratigraphic-event zonal markers.

halves of core sections. The ODP core-orientation scheme arbitrarily designates the X-axis as the horizontal (in situ) axis radiating from the center of the core through the space between a double line inscribed lengthwise on the working half of each core liner (Fig. 10). The natural remanent magnetization (NRM) and remanence measurements after 5, 10, 15, and 20 mT AF demagnetization were routinely measured at intervals of 10 cm.

Low-field Susceptibility

Whole-core susceptibility values are relatively rapid to measure, are nondestructive, and provide a rough indication of the amount of magnetizable material in the sediment, including ferrimagnetic and paramagnetic constituents. The instrument was set to the low sensitivity range (1.0) in the SI mode, and measurements usually were performed every 5 cm, depending on the available time for shipboard measurements. The susceptibility data were archived in raw instrument meter readings. To convert these values to susceptibility units, one must multiply by 0.63, calculated from the manufacturer's manual, to compensate for the 0.77 ratio of core diameter (68 mm) to coil diameter (88 mm). An additional multiplier of 10^{-5} is necessary for completing the conversion to volume-normalized SI units. These factors were checked vs. the values expected for distilled water. The meter was placed at zero with each section, but no correction was made on board

the ship for the instrument's baseline drift that occurred when measuring each section's susceptibility profile. However, the necessary parameters were recorded and will be processed on shore.

Magnetic Anisotropy

AMS measurements were performed on discrete samples to determine the geometry of the mineral fabrics found in the Leg 156 cores. The KLY-2 device determines the magnetic anisotropy tensor from measurements of magnetic susceptibility in 15 orientations, with the eigenvalues and eigenvectors of the tensor representing the magnitude and orientation of the principal susceptibility axes ($k_{max} > k_{int} > k_{min}$). Based on previous work from Leg 110 (Hounslow, 1990), most samples from Leg 156 should have AMS, which is controlled by paramagnetic clay minerals. Within the ash layers, AMS will likely measure magnetite fabrics.

Core Orientation

Reorientation of the rotated portions of XCB cores was also accomplished by using paleomagnetic results. Discrete samples, or portions of core, were AF demagnetized, and the characteristic remanence direction was calculated using principal component analysis. The declinations of the characteristic directions then were rotated to

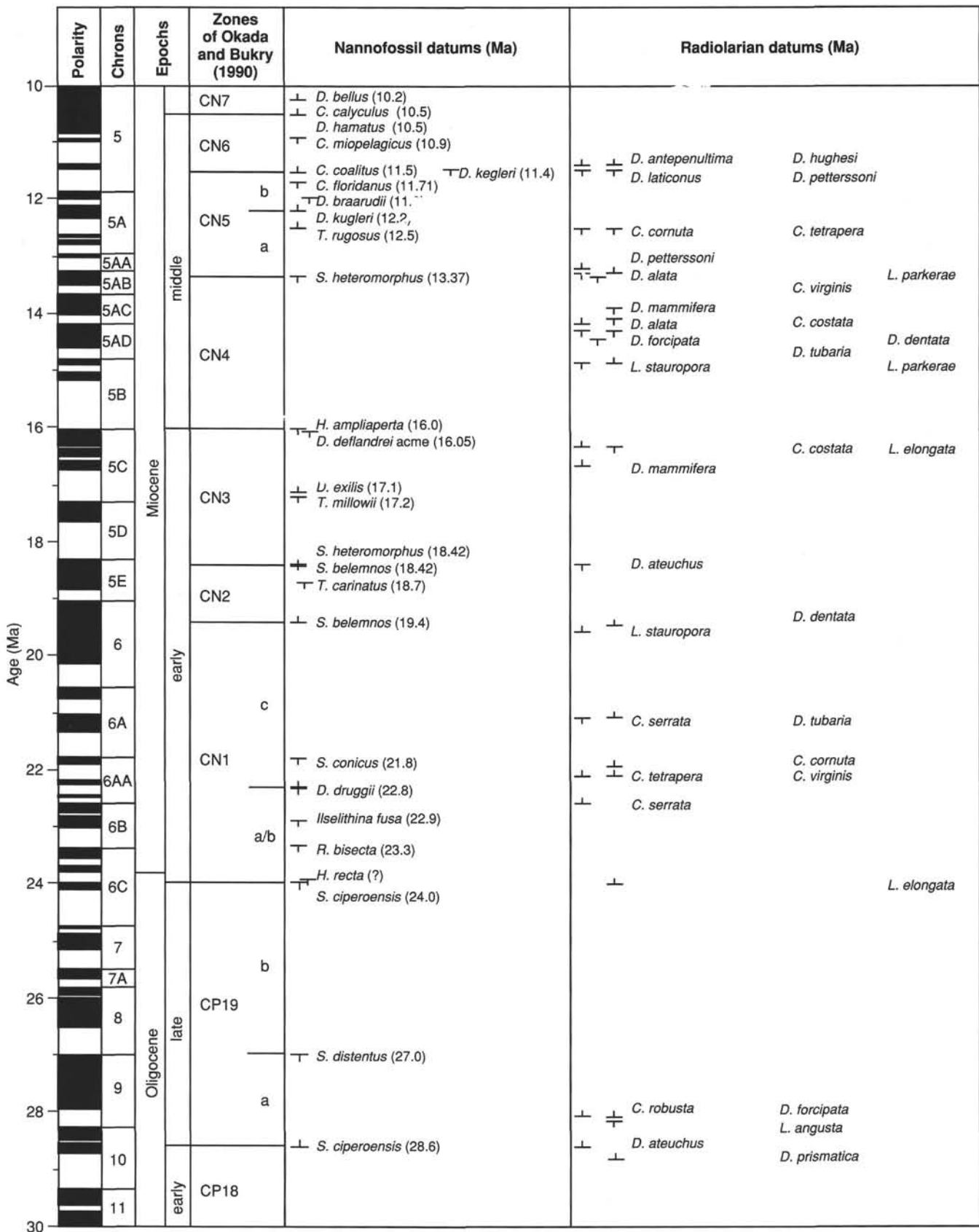


Figure 9 (continued).

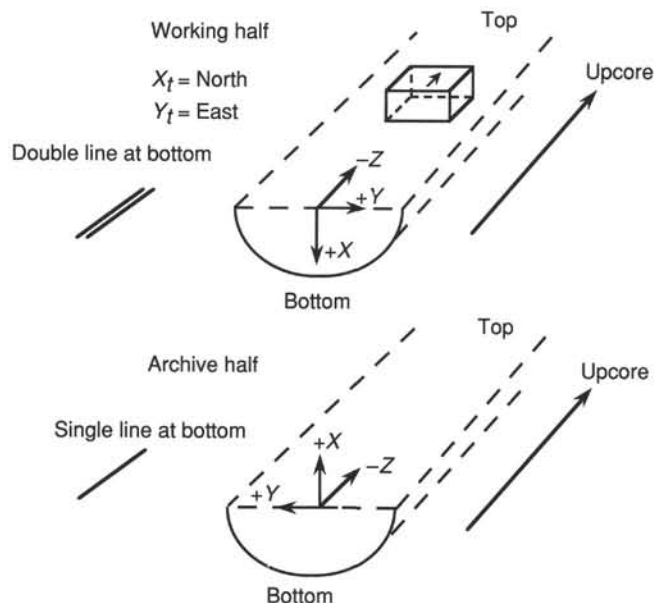


Figure 10. Core-orientation conventions for split-core sections and discrete samples.

360° (for normal polarity) or 180° (for reversed polarity). In general, reorientation of structural and magnetic fabric data using paleomagnetic results was highly successful during Leg 156.

Magnetostratigraphy

Whenever possible in the site chapters, we offer an interpretation of the magnetic polarity stratigraphy using the magnetic polarity time scale of Cande and Kent (1992). Two additional short geomagnetic features, observed with sufficient regularity that these may make useful stratigraphic markers for regional/global correlations, are the Blake feature at about 0.11 Ma in the Brunhes and the Cobb Mountain event at about 1.1 Ma. For the upper part of the time scale (roughly Pliocene–Pleistocene), we have used the traditional names to refer to various chronozones and subchronozones (e.g., Gauss, Jaramillo).

ORGANIC GEOCHEMISTRY

Shipboard chemistry during Leg 156 was conducted to provide real-time monitoring of hydrocarbon gases for safety reasons and for the initial characterization of the content and type of gases and organic matter in sediments. These analyses provide a basis for the preliminary site summaries and background for more detailed shore-based studies.

Hydrocarbon Gases

During Leg 156, the compositions and concentrations of hydrocarbons and other gases in the sediments were monitored generally at intervals of one to five samplings per core using the headspace (HS) method.

In the HS method, gases released by the sediments after core recovery were analyzed by gas chromatography (GC) with the following technique: immediately after retrieval on deck, a calibrated cork borer was used to obtain a measured volume of sediment from the end of a core section. The sediment, usually about 5 cm³, was placed in a 21.5-cm³ glass serum vial that was sealed with a septum and metal crimp cap. When consolidated or lithified samples were encountered, chips of material were placed in the vial and sealed. The vial was then heated to 60°C in an oven and kept at this temperature for 30 min prior to gas analysis. A 5-cm³ volume of the headspace in the vial was extracted with a standard glass syringe for each GC analysis.

The gas chromatograph (Hach-Carle AGC series 100, Model 211) has the following characteristics: sample introduction is via a 1.0-cm³ sample loop with manual column backflush; the chromatographic column used was a 0.32-cm × 1.8-m stainless steel tubing packed with 80% Poropak N and Poropak Q (80/100 mesh). A flame ionization detector (FID) was used, and separation of methane, ethane, ethene, and propane was performed at an isothermal condition (90°C), with helium used as the carrier gas. A Hewlett-Packard (HP) ChemStation was used to collect data and to calculate concentrations from peak areas and response factors from calibrations using external standards.

Bitumen Analyses (C₁₅₊ Hydrocarbons)

Hydrocarbons extracted from dry homogenized sediments using organic solvents were concentrated in normal hexane and analyzed by capillary gas chromatography.

Different methods were applied at Site 948 and Site 949 with respect to drying and solvent extraction of samples. From the results obtained at Site 948 a slight contamination of samples during freeze-drying was suspected. Exchanging the oil of the freeze-drier vacuum pump resulted in a distinct contamination of a few samples. Therefore, samples from Site 949 were dried in an oven at 40°C. Solvent extraction was carried out using a 1:1 mixture of normal hexane and methanol at Site 948 and a 7:3 mixture of dichloromethane and methanol at Site 949. The reason for changing the organic solvents was that the GC-grade methanol was available only at Site 948. A few experiments with both extraction methods produced similar results for identical samples.

Apart from the differences mentioned, the sample preparation and extraction procedures were the same at both sites. The sediment samples were gently ground in an agate mortar, and about 500 mg of each was weighed out and transferred into 2-dram screw-capped vials. Organic solvents (normal hexane/methanol or dichloromethane/methanol, 4 mL) were added, and the vial was kept in an ultrasonic bath for about 4 hr, during which the suspension was shaken occasionally. The clear supernatant solution was pipetted into a second vial, and the extraction was repeated with another 2-mL aliquot of *n*-C₆H₁₄. The combined extract was evaporated to dryness under nitrogen blow-down at about 40°C, then taken up in *n*-hexane to a volume of 30 μL. A 5-μL sample was then injected using normal GC protocol. Hydrocarbons were identified by comparison of retention times with those of authentic standards. The final quantification of the results was based on the weight of dry sediment and the aliquot used in the injection. Solvent blanks were also analyzed.

Hexane-soluble organic material was analyzed by GC-FID using a capillary column and split injection. Helium was used as the carrier gas. Operating conditions for this instrument were as follows:

1. Column: HP Ultra 1 (cross-linked methyl silicon gum), 50 m × 0.2 mm × 0.11 μm film thickness.
2. Conditions: He, 400 kPa; air, 200 kPa; and H₂, 150 kPa.
3. Temperatures: injector, 275°C; detector, 300°C; temperature program, initial at 30°C for 3 min, 10°C/min to 220°C, 4°C/min to 300°C, and then isothermal for 15 min.

Organic Matter

Organic Carbon

The total organic carbon content (TOC) of the sediments was determined by Rock-Eval TOC (explained below) or by the difference between carbonate carbon, determined with the Coulometrics Model 5030 carbonate carbon apparatus, and the total carbon value, determined by the Carlo Erba Model NA 1500 NCS analyzer. A description of the Coulometrics instrument and procedure can be found in the "Inorganic Geochemistry" section (this chapter).

Organic Matter Type (Pyrolysis Methods)

Dry homogenized sediments (100 mg) were analyzed using the Delsi-Nermag Rock-Eval II plus TOC. This system uses a whole-rock pyrolysis technique to identify the type and maturity of organic matter and to detect petroleum potential and oil shows in sediments, as described by Espitalié et al. (1985a, 1985b, 1986).

The Rock-Eval system involves a graduated temperature program that first releases volatile hydrocarbons at 300°C for 3 min, and then releases hydrocarbons from thermal cracking of kerogen as the temperature increases at 25°C/min from 300° to 600°C. Four parameters characterizing the organic matter are determined:

1. S_1 : The amount of free hydrocarbons (bitumen) in the sample (milligrams of hydrocarbons per gram of rock) recorded at pyrolysis temperatures below 300°C.
2. S_2 : The amount of hydrocarbons generated through thermal cracking of the kerogen as the sediment is heated at 25°C/min from 300° to 550°C during pyrolysis (cycle 1). S_2 is an indication of the quantity of hydrocarbons that could be produced in this rock, should burial and maturation continue.
3. S_3 : The quantity of CO_2 (milligrams of CO_2 per gram of rock) produced from pyrolysis of the organic matter at temperatures between 300° and 390°C is detected by the thermal conductivity detector (TCD) and recorded during cooling.
4. T_{max} : Maturity of the organic material assessed by the temperature at which a maximum release of hydrocarbons from cracking of kerogen occurs during pyrolysis (top of the S_2 peak).

The Rock-Eval data can also be interpreted for type of organic matter by the hydrogen index $[(100 \cdot S_2)/TOC]$, oxygen index $[(100 \cdot S_3)/TOC]$, and the S_2/S_3 ratio. The first two parameters are normally referred to as HI and OI, respectively. Rock-Eval pyrolysis is considered to be unreliable for samples having less than 0.5% TOC (Katz, 1983; Peters, 1986), although a correction procedure has been described for estimating matrix effects and obtaining reliable values on samples having lower amounts of TOC (Espitalié, 1980).

INORGANIC GEOCHEMISTRY

Sampling and Chemical Analyses of Interstitial Water

Shipboard interstitial-water analyses were performed on 7- to 40-cm-long whole-round sections that were cut and capped immediately after the core arrived on deck. The whole-round samples were usually taken from the bottom of Section 3, 4, or 5 of every core with sufficient recovery. Interstitial waters were retrieved by applying pressure to the sediment using a titanium squeezer (Manheim and Sayles, 1974). Before squeezing, the sediment was immediately extruded from the whole-round core liner, the surface was carefully scraped to remove potentially contaminated exteriors, and the cleaned sediment was placed into a titanium squeezer atop a Whatman No. 1 filter previously rinsed in high-purity water to remove processing acids. A second filter paper and a titanium piston were placed on top of the sample in the cylinder, and up to 205 MPa (30,000 psi) pressure was applied with a hydraulic press. Interstitial water was collected into a plastic syringe attached to the bottom of the squeezer assembly and filtered through a 0.45- μ m polycarbonate filter. Samples were stored in plastic vials pending shipboard analyses. Aliquots for future shore-based analyses were placed in acid-washed plastic tubes and glass ampoules and heat-sealed.

Interstitial-water samples were analyzed routinely for salinity as total dissolved solids with a Goldberg optical hand-held refractometer (Reichert); for pH and alkalinity, by Gran titration with a Brinkmann pH electrode and a Metrohm autotitrator; for dissolved chloride, calcium, and magnesium concentrations, by titration; and for silica, phosphate, and ammonium, by spectrophotometric methods with a Milton Roy Spectronic 301 spectrophotometer, following the analyti-

cal techniques described by Gieskes et al. (1991). International Association of Physical Sciences Organizations (IAPSO) standard seawater was used for calibrating most techniques. The reproducibility of these analyses, expressed as 1 σ standard deviations of means of multiple determinations of IAPSO standard seawater or of a standard, are alkalinity, <1.5%; chloride, <0.3%; calcium, <0.5%; magnesium, <0.5%; silica, <3%; and phosphate and ammonia, 4%. At all sites, sodium was determined using charge balance calculations where $\Sigma(\text{cation charge}) = \Sigma(\text{anion charge})$.

Potassium and sulfate were analyzed by ion chromatography (IC) using the Dionex DX-100. The reproducibility of these analyses, expressed as 1 σ standard deviations of means of multiple determinations of IAPSO standard seawater, are potassium, <2%; and sulfate, ~1%. Potassium was also analyzed by atomic emission spectrometry, which provides similar precision to IC, of <2% relative error but higher accuracy. Only these data are therefore reported. Calcium and magnesium were also routinely determined using the IC, but those results are not reported because titrations (calcium and magnesium) provided more accurate and precise results. For calcium, a precision of ~2% (1 σ standard deviation of repeat IAPSO determinations/published IAPSO concentration) of IAPSO standards was obtained with the IC, as opposed to <0.5% by titration. For magnesium, the precision was low, ~9% with the IC, and also compared unfavorably with <0.5% relative error by titration. The IC results, however, were a useful check on the general trends of potassium, calcium, and magnesium. Although the IC method is not optimized for the high concentrations of sodium and chloride of marine interstitial waters relative to the concentrations of the other constituents, they were routinely analyzed with the other cations and anions, respectively. Even for sodium and chloride, the precision with the IC is ~1% for Cl and <2% for Na, but the accuracy is low. However, these IC results did provide a useful check on the general trends of the depth profiles.

In addition to potassium, lithium and manganese concentrations were determined using flame spectrophotometric techniques with a Varian SpectrAA-20 atomic absorption unit. Lithium standards and some samples were determined on 1/5 diluted aliquots in nanopure water; more concentrated samples were diluted 1/10. As with potassium, lithium concentrations were determined by emission using an air-acetylene flame. Manganese concentrations were determined on 1/5 to 1/100 diluted aliquots with lanthanum chloride used as an ionization suppressant. Manganese was determined by atomic absorption using an air-acetylene flame. Except for Mn, standards for flame spectrophotometric techniques were matched in matrix composition to the samples. The reproducibility of these techniques, expressed as 1 σ standard deviations of means of multiple determinations of IAPSO standard seawater or of a standard treated as samples, are lithium (<1) and manganese (<2).

Chemical data for interstitial waters are reported in molar units.

Inorganic Carbon

Inorganic carbon was determined using a Coulometrics 5011 carbon dioxide coulometer equipped with a System 140 carbonate carbon analyzer. A known mass, ranging from 40 to 50 mg, of freeze-dried (dedicated carbonate samples) or oven-dried (physical property samples), ground sediment was reacted in a 2N HCl solution. The liberated CO_2 was titrated in a monoethanolamine solution with a colorimetric indicator, while the change in light transmittance was monitored with a photo-detection cell. The percentage of carbonate was calculated from the inorganic carbon content, assuming that all carbonate occurs as calcium carbonate,

$$\%CaCO_3 = \%C_{inorg} \times 100/12.$$

The precision of these analyses, expressed as 1 σ standard deviations of means of multiple determinations of a pure carbonate standard, is <1%.

Elemental Analysis

Total nitrogen, carbon, and sulfur contents of sediment samples were determined using an NCS analyzer, Model NA 1500 from Carlo Erba Instruments. Mixtures of vanadium pentoxide and crushed freeze-dried samples (~5 mg) were combusted in an oxygen atmosphere at 1000°C, converting total (organic and inorganic) carbon to CO₂, sulfur to SO₂, and nitrogen to NO₂. The NO₂ was reduced to N₂ using copper. The gases then were separated by gas chromatography and measured with a thermal conductivity detector. The precision of these analyses, expressed as 1 σ standard deviations, is 2% to 3%. Total organic carbon (TOC) was calculated by difference between total carbon (TC) from the NCS analyzer and inorganic carbon (IC) from the coulometer as

$$\text{TOC} = \text{TC} - \text{IC}.$$

CORE PHYSICAL PROPERTIES

Introduction

General Objectives

The principal objectives for the physical properties group are closely connected to the main scientific and operational goals of this cruise (Shiple et al., 1994). These can be grouped together as follows:

1. Physical properties, including porosity and mechanical and acoustic variations of sediments across the décollement zone, and other large-scale structural discontinuities;
2. Evolution of physical and deformational properties of sediments during accretion;
3. Integration of core physical property data with physical parameters derived from standard and special logging operations and experiments (LWD, conventional, and shear-wave VSP and WSTP).

A large number of whole-round core samples was taken during the cruise for shore-based testing of consolidation, permeability, and acoustic parameters. Standard shipboard measurements of physical properties included nondestructive, whole-core, MST measurements. Thermal conductivity was measured using the needle probe method when the sediment was soft enough to allow us to insert the needles smoothly into whole-round sections at discrete intervals (one every second section). Index properties (bulk density, grain density, dry bulk density, water content, and porosity), undrained shear strength, electrical resistivity, and compressional- and shear-wave velocities were measured on samples from split core sections.

Sampling Strategy

To accommodate these general objectives, the sampling program for physical properties was planned so as to fulfill several requirements:

1. To provide a comprehensive record of recovered core properties. Whole-core sections were scanned with the MST before being split. Physical property samples were then selected from the split cores. An average of two samples per section was chosen to represent the dominant lithology. Additional samples were selected to represent intervals of unusual lithology or structure.
2. To cross-correlate shipboard analyses. Samples were selected in conjunction with sedimentologists and structural geologists to identify features of interest. Most physical properties were analyzed on common or adjacent sample intervals. Dried samples from index properties were forwarded to the chemistry laboratory for carbonate analyses, and splits from the dried portion of these were used for bulk X-ray-diffraction (XRD) mineralogical determinations and total carbon measurements. Samples for shore-based XRD and grain-size studies were selected adjacent to physical properties samples.

3. To calibrate standard wireline and LWD logs. Bulk density, porosity, acoustic velocity, and thermal conductivity from core samples provide identifying characteristics for interpreting logs.

4. To facilitate cross-correlation with sections drilled during DSDP Leg 78A and ODP Leg 110 in this area. Magnetic susceptibility was measured on whole-round sections at intervals of 5 cm to enable us to correlate stratigraphic horizons with adjacent holes.

Laboratory Measurements

Index Properties

Index properties (bulk density, grain density, water content, porosity, dry density, void ratio) were calculated from measurements of wet and dry masses and wet and dry volumes on samples of approximately 10 cm³. Sample mass was determined to a precision of ± 0.01 g using a Scitech electronic balance. The sample mass was counterbalanced by a known mass, and multiple measurements were averaged to reduce effects of ship heave. Volumes were determined using a Quantachrome penta-pycnometer, a helium-displacement pycnometer. The pycnometer measures volumes to a precision of about ± 0.02 cm³. Volume measurements were repeated until two close measurements yielded volumes within 0.02 cm³ of each other. An initial purge time of 3 and 1 min for repeated runs was used. A reference volume was run with each group of four samples during all the tests. The standard was rotated among cells to check for systematic error.

The sample tare (beaker) masses were checked during the first week of the cruise. The ODP physical properties database was updated with these corrected values.

Water content, bulk density, porosity, grain density, dry density, and void ratio were determined following the procedures outlined in Blum (1994). These procedures comply with the American Society for Testing and Materials (ASTM) designation (D) 2216 (ASTM, 1989). Bulk density, grain density, and porosity are computed from the wet and dry masses of the sample and from one of two volume measurements, including corrections for pore-water salt precipitation. In Method B, the volume of the wet sample is used, while in Method C, the volume of the dry sample is used (Blum, 1994). Grain densities obtained using Method C typically range from 2.60 to 2.75 g/cm³, with some exceptions in the most clay-rich lithologies. This is compatible with the average density of the constituent minerals (quartz, calcite, kaolinite, illite, montmorillonite). In contrast, the grain densities calculated by Method B are unrealistically high, varying from 2.85 to 3.30 g/cm³. Furthermore, bulk-density values from this method are higher on average than those from LWD gamma-ray densitometry at the same depth. This is contrary to what one would expect as a consequence of elastic rebound during unloading. The systematic error in the weight measurements was found to be less than 0.1% of the measured mass (based on calibration standards). The error that could result from assuming constant salinity and density for the pore fluid (1.024 g/cm³ for seawater) is small, unless the sample is dehydrated when the wet measurements are performed. Thus, a systematic error of a few percentage points for the measured wet volume is implied. This hypothesis still needs to be verified and, in fact, is inconsistent with values measured for pure distilled water, which are accurate within the instrument's resolution. This problem is not new and may account for the generally higher porosities obtained by Method B, compared with Method C, from previous cruises. We preferred, and presented, Method C for measuring grain density, porosity, and void ratio. We made an exception with the bulk density, however, as Method B is more direct. Results from both methods are presented in the tables, and results from the use of Method B are plotted in figures.

Multisensor Track

The MST incorporates the magnetic susceptibility meter (MSM), gamma-ray attenuation porosity evaluator (GRAPE), P-wave logger

(PWL), and natural gamma-ray (NGR) radiation sensor on a trade system for whole-round core measurements.

The GRAPE device measures bulk density at user-defined time intervals by comparing attenuation of gamma rays through the cores with attenuation through an aluminum standard (Boyce, 1976). Generally, the GRAPE data are most reliable in APC cores where core liners are completely filled with sediment. The raw values of bulk density were corrected for interstitial waters not having the same gamma-ray absorption coefficient as quartz (Boyce, 1976).

The PWL transmits 500-kHz compressional-wave pulses through the core at a rate of 60 kHz. The transmitting and receiving transducers are aligned perpendicular to the core axis. A pair of displacement transducers monitors the separation between the compressional-wave transducers. Variations in the outside diameter of the liner do not degrade the accuracy of the velocities; however, the PWL does not provide accurate measurements on cores thinner than the inner diameter of the core liner. Measurements are taken at intervals of 2 cm. Weak returns having signal strengths below a threshold value of 200 digital increments (out of a maximum of 255) were removed.

Magnetic susceptibility was measured on all sections at 5-cm intervals using the 0.1 range on the Bartington meter with an 8-cm-diameter loop. This close sampling was conducted to provide another measure for between-hole correlation.

Generally, the accuracy of GRAPE, PWL, and MSM measurements degrades in XCB sections, where the core is undersized and/or disturbed. However, the general downhole trends can be used for stratigraphic correlation.

Compressional-wave (P-wave) Velocimetry

During Leg 156, *P*-wave velocity measurements were obtained using two different systems, depending on the degree of lithification of the sediment. *P*-wave velocities were measured in softer sediment using a digital sonic velocimeter (DSV) (Mayer et al., 1987). Velocity calculation is based on the accurate measurement of the delay time of an impulsive acoustic signal traveling between two pairs of piezoelectric transducers that have been inserted into the split sediment cores parallel and orthogonal to the core axis. These transducers are firmly fixed to a steel plate, so that their separation remains constant when determining velocities. The longitudinal and transverse transducer separation is 8.5 and 4.5 cm, respectively.

The signal used is a 2- μ s square wave; the transducers have resonances at about 250 and 750 kHz. A dedicated microcomputer controls all functions of the velocimeter. The transmitted and received signals are digitized by a Nicolet 320 digital oscilloscope and transferred to the microcomputer for processing. The DSV software selects the first arrival and calculates sediment velocity. No correction for in situ temperature and pressure was applied to the reported velocity data.

The sampling interval was usually two per section. Periodically, the separation was precisely evaluated by running a calibration procedure in distilled water. A value of sound velocity in distilled water is determined (based on standard equations) for the measured temperature, while the computer calculates the transducer separation using the signal's traveltime.

The Hamilton Frame velocimeter was used to measure compressional-wave velocities at 500 kHz in discrete sediment samples (1) when induration made it difficult to insert the DSV transducers without making any perturbations around them, and (2) in indurated sediments when insertion became impossible. Samples were carefully cut with a double-bladed diamond saw from intact "biscuits." Each individual sample was measured three times: V_{pt} in longitudinal direction (i.e., propagation parallel to the core axis) and V_{pt1} and V_{pt2} in transverse direction (i.e., propagation in a horizontal plane normal to the core axis) with a 90° angle between both transverse measurements. To facilitate later reorientation of the transverse velocities using paleomagnetic techniques, a consistent naming convention was used for V_{pt1} and V_{pt2} with respect to the surface of the split core (Fig. 11).

Sample thickness was measured directly from the velocimeter-frame lead screw through a linear resistor output to a digital multimeter. Zero traveltimes for the velocity transducers were estimated by linear regression of traveltime vs. distance for a series of aluminum and lucite standards. Filtered seawater was used to improve the acoustic contact between the sample and the transducers. The DSV oscilloscope and processing software were used to digitize waveforms and to calculate velocities.

Shear-wave (S-wave) Velocimetry

S-wave measurements on split-core samples were attempted for the first time on an ODP cruise. The equipment and procedure described here were introduced specifically for this leg by a participating scientist, and are not part of the standard shipboard laboratory.

S-wave velocities were measured on unlithified sediment cores with "bender" transducers (Fig. 12A). These measurements were performed within 1 cm of the DSV *P*-wave measurements. Two measurements were performed, parallel and perpendicular to the core axis. The two transducers were inserted with bender elements collinear and about 10 mm apart (Fig. 12B). The transmitting transducer produces a shear wave that has been polarized perpendicular to its faces, which excites the receiving transducer. (The orthogonal bender elements in each transducer were redundant when the transducers were used in side-by-side mode.) The signal has a frequency of 1 to 2 kHz and was heavily contaminated by acoustic and electrical noise in the laboratory, so that 100 waveforms were summed before measuring travel-times. The input signal (10-V square wave, 16-ms half-period) is also summed and the traveltime measured with the oscilloscope cursors. Velocities in typical sediments are 20 to 200 m/s, so that travel-times of 0.1 to 1.5 ms were expected for transducer separations of 10 to 30 mm.

The transducers were fitted into a jig to ensure that separation was constant. Accurate first-break picking depends on correct grounding of the apparatus to remove signal-generated electrical transients. The metal core track was connected to the oscilloscope ground and a copper pin, also connected to the oscilloscope ground, was inserted into the core near the point of measurement.

For stiffer sediments, measurements were performed on the specimen used for the Hamilton Frame *P*-wave measurements. The specimen, wrapped in thin plastic film to prevent desiccation, was placed between the two transducers in a modified vise (Fig. 12C). For these stiffer specimens, the transducer blades indented but did not penetrate the sediment. Shear-wave traveltimes for waves polarized in two orthogonal directions were measured between each of the three pairs of faces (six measurements in all). Transducer separations were determined by measuring the separation of the end plates of the vise with calipers, then subtracting the length of the transducers. Again, the vise and the specimen were connected to the oscilloscope ground.

The S-wave measurements attempted on this cruise were plagued by a number of experimental problems: The wavelength of up to 80 cm in specimens less than 3 cm long causes traveltime errors; in fact it may not be clear whether traveltime or finite strain effects are measured. Measuring the vise end-plate separation with calipers caused systematic underestimation and an error of up to 0.2 mm. Calibrating the transducers was difficult for lack of reference specimens with unvarying dimensions and velocity. Therefore, the results should be viewed with caution.

Natural Gamma Rays

Emission of natural gamma rays was measured routinely at 15, 75, and 135 cm in each section, while the core boat stopped for 30 s. The area of influence for the four NGR sensors is about ± 10 cm from the points of measurements along the core axis. Data were recorded in five spectral windows similar to those of the Schlumberger downhole logging (NGT) tools (Table 6). Total counts were also recorded and are the sum of all window counts (Hoppe et al., in press).

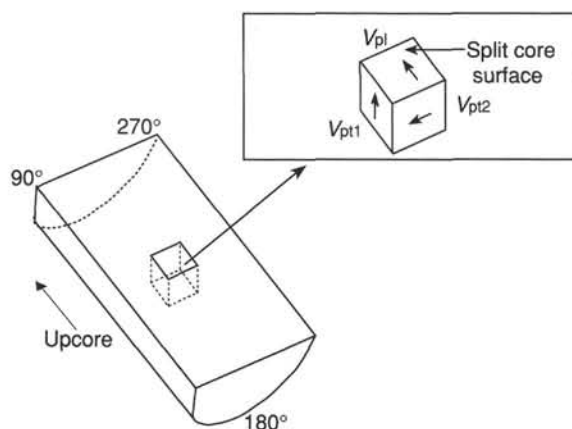


Figure 11. Schematic representation of orientation and naming conventions used for Hamilton Frame velocimeter samples. See text for explanation of abbreviations.

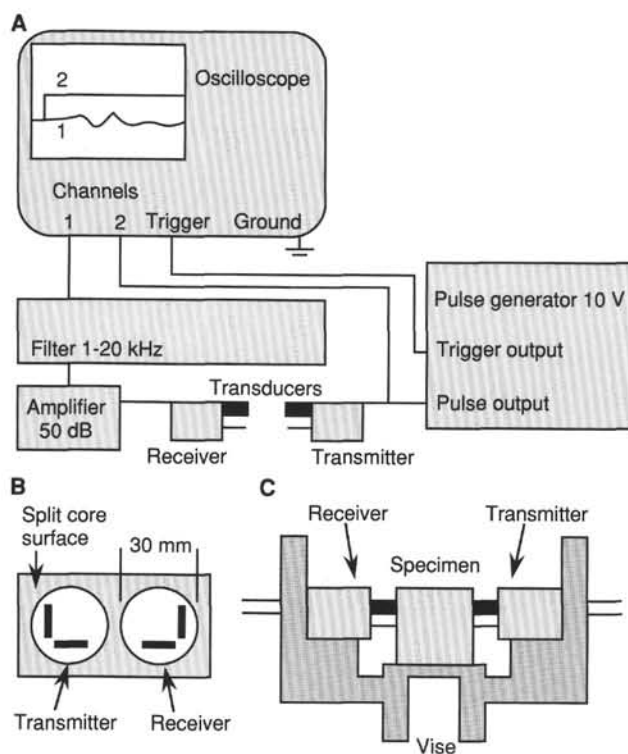


Figure 12. A. Shear-wave measurement apparatus: instrument configuration. B. Side-by-side transducer configuration. C. End-by-end transducer configuration.

Before starting measurements, we adjusted the four sensor gains so that the combined potassium peak was as sharp as the individual peaks when the other three were disabled. The multichannel analyzer then was calibrated by assigning certain channels to the characteristic energies of ^{40}K and the main peak of ^{232}Th . We found that the calibration was not linear over the entire spectrum from 0 to 3 MeV (the first channel was assigned a negative energy). However, because we used the readily available KCl (chemistry laboratory) and Th (Schlumberger engineer) standards for calibration, the most informative interval of the spectrum was as nearly linear as possible. The previous calibration performed before Leg 149 used two peaks at 0.12 and 1.48 MeV from the europium spectrum, which assigned an energy 0.2 MeV too high to the Th peak (Table 6). Although the effect of our recalibration on the routinely used total counts is negligible, the mismatch of the

Table 6. MST NGR spectral windows and their multichannel analyzer definitions before and after recalibration during Leg 156.

Window number	Energy range (MeV)	MCA Range 1 (channel number)	MCA Range 2 (channel number)	Characteristic isotope of energy window
W1	0.2–0.5	0147–0344	0185–0373	
W2	0.5–1.1	0346–0741	0374–0751	
W3	1.1–1.59	0743–1065	0752–1059	^{40}K
W4	1.59–2.0	1067–1336	1060–1317	Main ^{238}U peak
W5	2.0–3.0	1338–1997	1328–1948	Main ^{232}Th peak

Notes: MCA Range 1 is based on Leg 149 two-peak europium calibration. MCA Range 2 is based on Leg 156 two-peak ^{40}K - ^{232}Th calibration.

Th peak is significant when using the spectral information. Thus, we strongly recommend using K and Th for future recalibrations.

Background radiation was first measured for air and for a core liner filled with distilled water to determine which one should be used. Ten tests of 10 min counting time were run for each, and these showed that the water background was more realistic, as subtracting the higher air background from low-count data resulted in incidents of negative counts. A set of 460 measurements, 10/hr for two days, was conducted. Counting time was 30 s, to compare those statistics with the core measurements. The results (Table 7) indicate that standard deviations for high-energy, low-count windows W3 to W5 are high, relative to the mean values, whereas for total counts, the error introduced by background variations is small. One should be cautious therefore when interpreting variations in the contents of K, U, and Th from 30-s measurements. Finally, the mean background values from Table 7 were then subtracted from the data, after normalizing the counts to counts per seconds (cps).

Undrained Shear Strength

The undrained shear strength, S_u , of the sediment was determined using the ODP motorized miniature vane shear device, following the procedures of Boyce (1976). The vane rotation rate was set to 90°/min. Measurements were performed only in the fine-grained, soft units. The vane used for all measurements has a 1:1 blade ratio with a dimension of 1.27 cm. A range of springs of various strengths were available. These springs were calibrated prior to Leg 156.

The instrument measures the torque and strain at the vane shaft using a torque transducer and potentiometer, respectively. The shear strength reported is the peak strength determined from the torque vs. strain plot. In addition to the peak shear strength, the residual strength was determined from the same plot where the failure was not dominated by cracking of the sample (Pyle, 1984).

When analyzing vane tests, one assumes that a cylinder of sediment is uniformly sheared about the axis of the vane in an undrained condition, with cohesion as the principal contributor to shear strength. Departures from this assumption include (1) progressive cracking within and outside of the failing specimen, (2) uplift of the failing core cylinder, (3) drainage of local pore pressures (i.e., the test can no longer be considered to be undrained), and (4) stick-slip behavior. Evidence of cracking was noted in the “Comments” section of the results file.

Electrical Resistivity

The Wayne-Kerr precision component analyzer was used to measure resistivity with a four-electrode method: two outer electrodes inject an alternating current while two inner electrodes measure the resulting potential difference. The apparent resistance, U/I , is proportional to the resistivity of the medium.

The probes consisted of four tiny needles (Wenner array) spaced 3 mm apart and were fabricated from standard gold-plated electronic connector strips. Electrical resistivity was usually measured twice per

section near the index property samples. Several measurements were performed in both longitudinal and transverse directions to evaluate anisotropy.

Because the quality of the contact between the needles and the core or calibrating fluid tends to degrade with time (as gold-plating is removed from the pins by abrasion?) and because the area of contact depends on how the probe is inserted, calibrations were performed before and after each series of measurements. Assuming that the pore fluid has the same conductivity as seawater, the formation factor was computed as the ratio of the resistance measured in the core and the resistance measured in seawater and corrected for the temperature difference.

The temperature of the cores was generally $22^\circ \pm 0.5^\circ\text{C}$, but the temperature of the calibrating fluid was usually closer to the ambient laboratory temperature (23° to 26°C). The formula giving the conductivity of seawater:

$$c = 2.803 + 0.0996 T (\text{C}) \Omega^{-1}\text{m}^{-1}$$

is taken from the shipboard resistivity manual. The resulting correction of the calibrations is about 10%. When the temperature measurements were not made, average temperatures were used.

Calibration was done with standard seawater. To improve reproducibility and the quality of the calibration, a modified probe was used for all measurements in Holes 949A and 949B. A plexiglass guard was glued to the needles with epoxy to ensure that the areas of contact with the sediment and with the calibrating fluid were the same. Calibration was done with seawater before and after each core measurement (Table 8). The geometrical factor, d , is determined such that $r = R \cdot d$, where R is measured resistance and r is resistivity. The theoretical value of this factor for the apparatus is 16.7 mm for 2.67-mm spacing between adjacent needles. The probe drift at Site 949 was fit by a polynomial regression (Fig. 13):

$$1/d = 82.759 - 0.13361 \cdot n + 1.11758e-4 \cdot n^2 + 1.0737e-6 \cdot n^3,$$

where n is the measurement number.

The initial increase in d probably resulted from abrasion of an epoxy film on the needles, left over from construction. The later decrease may result from removal of the gold-plating and subsequent degradation of the contact. The remaining dispersion is indicative of the precision of the measurement. Three consecutive measurements with anomalously high resistance resulting from insufficient probe cleaning were discarded, yielding a standard error of the interpolated fit to the calibrated data (65% confidence interval) of $\pm 3.8\%$.

An modified probe was used on Core 156-949C-7R with good results. The needles were waxed before gluing to prevent formation of the epoxy film, and the wax was removed before measurements were taken.

Thermal Conductivity

The thermal conductivity of cored material was measured in locations in every section using the needle probe method, in full-space configuration for soft sediments (Von Herzen and Maxwell, 1959). All measurements were performed after the cores had equilibrated to the laboratory temperature. Data are reported in units of $\text{W}/(\text{m}\cdot\text{K})$ and have an estimated error of 5% to 10%.

Needle probes containing a heater wire and a calibrated thermistor were inserted into the sediment through small holes drilled in the core liners before the sections were split. Data were acquired using a Thermcon-85 unit interfaced to an IBM-PC-compatible microcomputer. This system allowed up to five probes to be connected and operated simultaneously.

At the beginning of each test, temperatures in the samples were monitored without applying a heater current until the background thermal drift was determined to be less than $0.04^\circ\text{C}/\text{min}$. Once the samples were equilibrated, the heater circuit was closed and the temperature rise in the probes was recorded. Thermal conductivities

Table 7. MST NGR background radiation.

	Total	W1	W2	W3	W4	W5
Mean	8.05	4.61	2.12	0.72	0.24	0.36
Std. dev.	0.52	0.40	0.27	0.16	0.09	0.11
Std. dev./mean (%)	6.49	8.66	12.87	22.62	36.43	31.39

Notes: A set of 450 measurements, 30 s each, was conducted during a 48-hr period, with distilled water core in apparatus. W = window.

were calculated from the rate of temperature rise while the heater current was flowing.

After the heater has been on for about 60 s, the needle probe response is very close to that of a line source with constant heat generation per unit length. Temperatures recorded during a time interval of 60 to 240 s were fitted with the least-squares technique to the appropriate equation:

$$T(t) = (q/4\pi k) \cdot \ln(t) + L(t),$$

where k is the apparent thermal conductivity, T is temperature, t is time, and q is the heat input per unit length of wire per unit time. The term $L(t)$ describes a linear change in temperature with time and includes the background temperature drift and any linearity that results from instrumental errors and the geometrical inadequacies of the experiment. These inadequacies include the finite length of the probe and sample.

All measurements were corrected for a linear offset between measured and true thermal conductivities, determined from a series of tests with standards of known conductivities (Table 9).

DOWNHOLE LOGGING

Introduction

The Lamont-Doherty Earth Observatory-Borehole Research Group (LDEO-BRG), in conjunction with Schlumberger Well Logging Services and Schlumberger-Anadrill Drilling Services, provides the geophysical well logging aboard the *JOIDES Resolution*. Downhole logs allow direct determination of physical and chemical properties of formations adjacent to the borehole. Interpretation of these continuous, in situ measurements yields mineralogic, lithologic, stratigraphic, and geophysical characterizations of the site. Where incomplete downhole core recovery has occurred, logging data may serve as a proxy for physical properties and sedimentological data. These data also complement the discrete measurements obtained from cores and offer several advantages over core-based analyses in that they are collected rapidly and represent continuous, in situ measurements of the formation.

During the first week of Leg 156, logging-while-drilling operations were conducted for the first time aboard the *JOIDES Resolution*. LWD allows for in situ measurements immediately after the drill bit penetrates a formation with instruments that are located at the base of the drill string. These measurements are performed before the borehole conditions deteriorate in response to drilling and coring operations. In addition, LWD measurements are performed while the drill string is moving, which reduces the chances of sticking and losing the bottom-hole assembly (BHA) in a swelling clay or sloughing hole situation. LWD operations were complemented by wireline logging following coring operations during Leg 156.

Well-logging Operations/Logging While Drilling

The drill string was configured with the LWD tools located directly above the drill bit (Fig. 14). Before the bottom of the drill string was lowered below the drill floor, the LWD tools were initialized. After total depth was drilled, the drill string was retrieved to the rig floor, and data were retrieved from each tool via a laptop computer.

Table 8. Resistivity probe calibration data.

Measurement number	Measured resistance (Ω)	Temperature (°C)	Standard resistivity (Ωm)	Geometrical factor, <i>d</i>		
				Measured (m)	Interpolated (m)	Error (%)
1	15.6	24.3	0.1915	0.0123	0.0121	1
10	16.1	23.2	0.1956	0.0121	0.0123	-1
11	16.1	24.5	0.1907	0.0118	0.0123	-4
20	15.2	22.2	0.1994	0.0131	0.0125	5
44	15.5	23.0	0.1963	0.0127	0.0130	-2
45	15.1	22.8	0.1971	0.0131	0.0130	1
63	15.0	23.7	0.1937	0.0129	0.0133	-3
64	13.9	23.7	0.1937	0.0139	0.0133	4
65	13.9	23.7	0.1937	0.0139	0.0134	4
70	14.5	25.5	0.1872	0.0129	0.0134	-4
91	14.2	23.6	0.1940	0.0137	0.0138	-1
99	15.0	23.1	0.1959	0.0131	0.0139	-7
100	14.2	22.8	0.1971	0.0139	0.0140	-1
125	14.0	23.1	0.1959	0.0140	0.0143	-2
126	13.0	22.6	0.1979	0.0152	0.0143	6
127	12.6	22.5	0.1983	0.0157	0.0143	9
144	13.9	23.2	0.1956	0.0141	0.0145	-3
145	13.6	23.8	0.1933	0.0142	0.0145	-2
174 ^a	15.6	23.5	0.1944	0.0125	0.0146	-17
175 ^a	15.5	24.2	0.1918	0.0124	0.0145	-18
176 ^a	16.6	21.3	0.2031	0.0122	0.0145	-19
204	14.1	22.2	0.1994	0.0141	0.0144	-2
223	14.5	22.7	0.1975	0.0136	0.0141	-4
224	13.3	23.7	0.1937	0.0146	0.0141	3
256	13.8	24.3	0.1915	0.0139	0.0135	3
257	14.0	24.4	0.1911	0.0136	0.0134	2
269	14.7	24.2	0.1918	0.0130	0.0131	-1
270	14.6	24.3	0.1915	0.0131	0.0131	0

^a Not used for interpolation.

Table 9. Calibration standards for thermal conductivity probes.

Standard	Known conductivity	Probe 332 (conductivity s.d.) ^a		Probe 344 (conductivity s.d.) ^a		Probe 346 (conductivity s.d.) ^a	
Black rubber	0.54	0.560	0.012	0.620	0.008	0.531	0.028
Red rubber	0.96	1.006	0.036	0.961	0.046	0.974	0.040
Macor	1.61	1.870	0.251	1.755	0.128	1.923	0.062

^a s.d. = standard deviation.

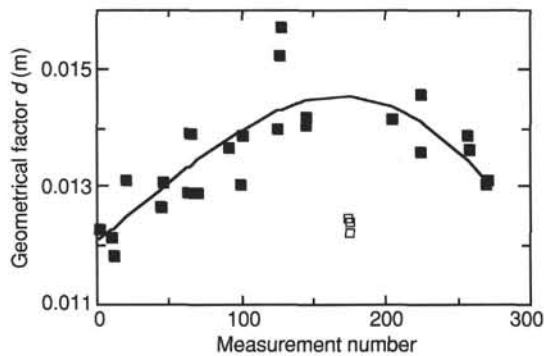


Figure 13. Variation of resistivity probe calibration with measurement number at Site 949. Solid squares represent successive calibrations. Open squares were not used in the polynomial regression. See text for discussion.

Description of LWD Tools

The Anadrill-Schlumberger tools used during LWD operations on Leg 156 were the compensated dual resistivity, including a spectral gamma-ray tool, and compensated density neutron tools (Anadrill-Schlumberger, 1993; Desbrandes, 1994). The LWD equipment is battery-powered and uses electronically erasable/programmable, read-

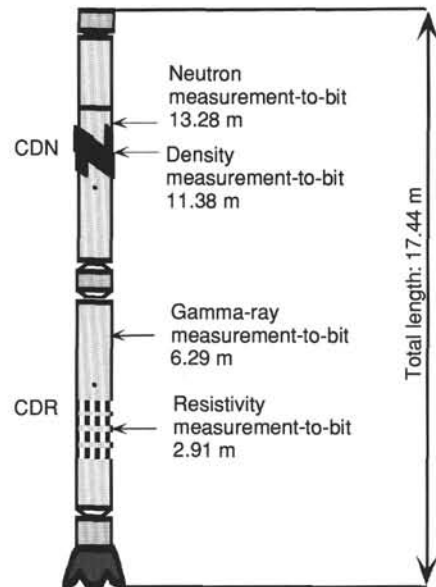


Figure 14. Positioning of CDR and CDN tools in the drill string during Leg 156 operations.

only memory chips (EEPROM) downhole for nonvolatile storage of data. The downhole data-acquisition systems are synchronized in time with an uphole system that monitors time and drillers' depth, as described below.

Compensated Dual Resistivity (CDR) Tool

The CDR tool is similar in principle to the conventional wireline induction tool that measures formation conductivity. Using a 2-MHz electromagnetic wave, two receivers detect the phase shift (shallow measurement) and amplitude attenuation (deeper measurement) of the transmitted signal. Two pairs of receivers and transmitters are used for borehole compensation in washouts and irregular boreholes.

The resistivity phase shift (R_{ps}) measurement is equivalent to the spherically focused log (SFL) on the induction tool. The average depth of investigation of the (R_{ps}) is 75 cm. The resistivity attenuation deep (R_{ad}) measurement is equivalent to the dual-induction medium measurement, with an average depth of investigation of 125 cm. The highest vertical resolution of these measurements is 15 cm.

A natural gamma-ray tool is integrated into the CDR tool. Under controlled penetration rates of approximately 15 m/hr, reliable spectral data may be obtained. Penetration rates during Leg 156 of greater than 45 m/hr degraded the resolution of the spectral data, but provided total gamma-ray counts similar to those recorded by the wireline tool.

Compensated Density Neutron Tool (CDN)

The CDN tool is similar in principle to the wireline compensated density/compensated neutron tools. The density section of the tool uses a 1.7-curie ^{137}Ce source for gamma rays in conjunction with two gain-stabilized scintillation detectors to provide a borehole compensated density measurement. Two types of interaction of gamma rays with the formation atoms are the basis for measurement of formation density and photoelectric effect, related to formation electron density and atomic number (lithology), respectively. At higher energy levels the number of Compton scattering collisions (change in gamma-ray energy by interaction with the formation electrons) is related to the formation density. Returns of low-energy gamma rays provide information about the photoelectric effect, which is primarily related to lithology. The density source and detectors are positioned behind holes in the fin of a full-gauge clamp-on stabilizer (Fig. 14). This geometry excludes mud from the path of the gamma rays, reducing the effects of an irregular borehole. The vertical resolution of the density and photoelectric-effect measurements is about 15 and 5 cm, respectively.

For the neutron-porosity measurement, fast neutrons are emitted from a 7.5-curie americium oxide-beryllium source. The quantities of hydrogen in the formation primarily control the rate at which the neutrons slow down to epithermal and thermal energies. The energy of the detected neutrons has an epithermal component because much of the incoming thermal neutron flux is absorbed as it passes through the 1-in. drill collar. Neutrons are detected in near- and far-spacing detector banks, located laterally above the source. The resolution of the tool under optimum conditions is about 34 cm.

Data from the CDN tool include apparent neutron porosity, formation bulk density, and photoelectric effect.

Depth Control

Unlike a wireline tool, the LWD tool records data in time and does not have an exact depth reference. The depth of the LWD tool is ultimately determined by matching its times with a system that independently records time and depth of the drill-string depth on the rig floor. Although LWD depth control for industry operations is well established, LWD operations aboard the heaving platform of the *JOIDES Resolution* required special attention to depth measurements. The LWD precision depth assembly (PDA) was carefully calibrated to the movements of drawworks. Procedures were established for setting

the drill-string heave compensator to the same point (mid-stroke) after every pipe connection during drilling. Fortunately, the ship's heave was small (less than ± 1 m) and, therefore, had a relatively small effect on depth control.

The PDA sensors consist of a depth encoder system, driven directly by the drawworks, and a hookload clamp line tensiometer that measures the weight of the drill string. The PDA data are recorded on a surface acquisition system and accurately track drill-string penetration and movement, determining the rate of penetration, hole depth, and bit position while drilling and tripping. The penetration of the drill string depends on sensing both weight on the drill bit and downward movement of the drill string. The combination of these two sensors, with precision synchronization of uphole and downhole clocks, allows one to correlate the surface time/depth data with the downhole time/measurement data files. A combination of these data files after downloading from the LWD tools yields depth/measurement data.

In addition to the depths determined by the LWD operation, depths were monitored independently by observers in the drilling shack. Depths recorded by the independent observers compared to those measured by the LWD system indicate that absolute depth errors are generally less than 3 m (see "Operations" section, this chapter, for further information on depths).

Well-logging Operations/Wireline Logging

Because the LWD tools did not provide information about sonic velocity or accurate spectral gamma-ray data, wireline logging was also conducted during Leg 156. Wireline operations followed immediately after coring and conditioning of the borehole for logging operations. A tool string (a combination of sonic and gamma ray plus either density or resistivity sensors) was lowered downhole on a seven-conductor cable to continuously monitor properties of the adjacent formation. Although the depths of investigation and vertical resolution are sensor-dependent, all properties are typically recorded at 15-cm intervals. The specific tool strings run in each hole are described in the "Downhole Logging" section of each site chapter. With the exception of the cement-bond tool, the open-hole logging tools used during Leg 156 have been described well in the "Explanatory Notes" chapter of the Leg 146 *Initial Reports* volume (Westbrook, Carson, Musgrave, et al., 1994). A detailed description of logging-tool principles and applications is provided in Dewan (1983), Schlumberger (1989), Serra (1984), and Timur and Toksöz (1985).

Cement-bond Log

Shot receivers for the vertical seismic profile are best located in areas where casing has been well cemented to the surrounding sediments. To evaluate the extent of cementation of casing, we ran Schlumberger's cement-bond tool (CBT). The CBT measures the amplitude and, hence, attenuation of a compressional wave generated and received in the tool. Amplitude decreases and attenuation increases with decreasing magnitude of cementation (Serra, 1984).

Log Analysis

The Schlumberger multitask acquisition and imaging system (MAXIS) allows for simultaneous recording and display of wireline-logging data. The MAXIS will output files as DLIS (digital log information standard) and ASCII data files, which are linked through the shipboard Ethernet, allowing shipboard scientists to access these data. Basic log interpretation is conducted aboard the ship; further analysis and interpretation are undertaken after the cruise at the LDEO Borehole Research Laboratory, at other research centers, and by shipboard logging scientists.

Shore-based Processing

Processing, quality control, and plotting of the logging data were performed by the LDEO-BRG, using Schlumberger "Logos" soft-

ware and additional programs developed by members of the BRG. Displays of most of these processed data appear with accompanying text at the end of the appropriate site chapters in this volume. Files of all processed logs (including high-resolution density data), sonic waveforms, and explanatory text are included on CD-ROM enclosed in the back pocket of this volume. A directory of the contents of the disk is found at the front of this volume.

Shore-based processing of data from each hole consisted of (1) depth adjustments of all logs to refer to seafloor datum at each hole, (2) corrections specific to certain tools, and (3) quality control and rejection of unrealistic values.

Specific tool corrections were performed on the gamma-ray data to account for changes in borehole size and for the composition of the drilling fluid.

In addition to the standard 15.24-cm sampling rate, bulk-density data were recorded at a sampling rate of 2.54 cm. The enhanced bulk-density curve is the result of the Schlumberger enhanced processing technique performed on the MAXIS system on board. While in normal processing short-spacing data is smoothed to match the long-spacing data, in enhanced processing this is reversed. In a situation where there is good contact between the high-temperature lithodensity tool (HLDT) pad and the borehole wall (low-density correction) the results are improved, because the short-spacing data have better vertical resolution.

Quality control was performed by cross correlation of all logging data. If the data processor concluded that individual log measurements represented unrealistic values, the choices were either to discard the data outright and substitute the null value of -999.25, or identify a specific depth interval containing suspect values that must be used with caution. Suspect values are noted in the text that accompanies all processed log displays. Quality control of the acoustic data was based on discarding any of the four independent transit-time measurements that were negative or that fell outside a range of reasonable values selected by the processor.

Locally, some intervals of log data appeared unreliable (usually due to poor hole conditions) and were not processed beyond what had been done on board ship. In general, a large (>12 in.) and/or irregular borehole affects most recordings, particularly those made with tools that require eccentricization (HLDT) and good contact with the borehole wall.

Synthetic Seismograms

Synthetic seismograms are generated from an impedance log, calculated from the velocity functions and bulk-density logs. The velocity and density logs were input to a program that generates an acoustic-impedance log (velocity \times density). The impedance log was converted to a reflectivity series and convolved with a wavelet derived from our three-dimensional seismic reflection data. Because the three-dimensional data set had been converted to depth, the usual step of converting the logs from depth to time prior to calculating synthetic seismograms was unnecessary.

CD-ROM Materials

The CD-ROM in the back of this volume contains both depth-shifted and processed logging data that has been provided by LDEO-BRG. The CD-ROM also contains shipboard measurements on cores collected on board *JOIDES Resolution* during Leg 156 (GRAPE, index properties, magnetic susceptibility, and natural gamma-ray data). CD-ROM production was done by LDEO-BRG, wireline logging operator for ODP.

The INDEX file contains a summary of all files loaded on the CD-ROM (see also Table of Contents, this volume.) The software documentation file in the GENERAL INFORMATION directory contains information about which software packages work best to import portable bitmap (PBM-8-bit binary) raster files. This file also included network sources for the graphics software and data compression information.

The README file contains information about whom to contact with any questions about the production of or data on the CD-ROM.

All of the ASCII files (basic logging and dipmeter files) are tab-delimited for compatibility with most spreadsheet and database programs. Holes that have long logging runs are often divided into TOP, MIDDLE, and BOTTOM directories. If the data were collected continuously, or if two or more sections were spliced together, the files would be in the SPLICED directory.

In the FMS-PBM subdirectory there are two subdirectories: 1:1, with maximum 10-m-long raster images at a 1:1 scale, and 1:10, with maximum 100-m-long raster images at a 1:10 scale. The raster image files are named according to their depth interval. The raster documentation files contain image file parameter information necessary for use with most graphics software packages.

HEAT FLOW

Scientific Objectives

Measuring heat flow was of primary importance to the main objectives of Leg 156 to characterize the hydrogeology of the toe of the Barbados accretionary complex. The thermal state of the sediments is strongly influenced by, and is thus a good indicator of, fluid flow in this setting. Pore-fluid chemistry is also strongly influenced by advection, and many geochemical tracers are at least an order of magnitude more sensitive to the effects of fluid flow than is formation temperature. In combination, analyses of thermal and chemical gradients provide indications of fluid flow over a wide range of velocities. Measuring heat flow requires assessments of in situ temperatures and thermal conductivities. This section describes the methods used during Leg 156 for collecting and analyzing in situ temperature data. Techniques used for in situ pore-fluid sampling during Leg 156 are covered in the "Inorganic Geochemistry" section (this chapter). Borehole-temperature logging tools used during Leg 156 are described in the "Downhole Logging" section (this chapter). Techniques for collecting and processing thermal conductivity data are described in the "Physical Properties" section (this chapter).

Water Sampler Temperature Probe (WSTP) Temperature Measurements

The WSTP is a hybrid of two other tools, the Uyeda temperature tool (Yokota et al., 1980) and the Barnes fluid sampler (Barnes, 1979, 1988). The original Uyeda temperature tool had a thin, stainless-steel probe that was pushed ahead of the bit into the undisturbed sediments at the bottom of a hole. The Leg 156 WSTP tip has a greater diameter than that of the Uyeda tool and can be configured with or without a fluid-sampling capability. When the probe tip is configured for temperature measurement only, the tip has a shorter time constant such that (1) the frictional heat pulse associated with insertion of the probe can be assumed to approximate more closely a line source of heat and (2) insertion of the instrument is less likely to fracture semilithified sediments. The development and use of different probe designs are described more fully in Shipboard Scientific Party (1992).

Recording of data was accomplished during Leg 156 using a modified Double Current Data Logger (DCDL), an instrument having a long history of modifications to improve stability, reliability, and calibrability. The DCDL contains one recorder and a clock, with a sampling interval of 4.369 s. The DCDL records thermistor resistances in RAM. These data are downloaded to an IBM-PC compatible following deployment for conversion to temperatures and additional processing.

In operation, the WSTP is mounted inside a core barrel and lowered down the drill pipe by wireline while the bit is held above the bottom of the hole. The tool is held briefly above the mud line to measure the temperature of bottom water. The tool is then lowered and latched into place, with the probe tip extending 1.1 m ahead of the bit. The drill string is lowered, and the probe is forced into the bottom of the hole. A collected delivery system allows the probe to retract back

up inside the bit, should the formation prove to be too hard to penetrate. With an APC/XCB BHA, the bit can be decoupled from the tool after penetration so that the probe will not be disturbed by ship's heave on the drill string.

The driller can continue to circulate fluid continuously during the station if necessary to keep the hole clear of fill, as circulation of cold bottom water in the hole has little influence on measured temperatures at times less than a few hours after drilling, so long as the probe penetrates at least 50 cm (Fisher and Hounslow, 1990). Insertion of the probe significantly disturbs formation temperatures, but as the instrument cannot be left in position to allow this disturbance to decay completely, extrapolation to thermal equilibrium is required. Data-reduction methods are described later in this section.

Thermistors used during Leg 156 were calibrated with an accuracy of better than 0.005°C over a range of 0° to 35°C using the Physical Oceanography calibration facility at WHOI during the spring of 1993. The large water bath used for these calibrations was instrumented with a sensor that was itself calibrated at the U.S. National Institute of Standards and Technology. Digital resolution of the DCDL is nominally 0.05°C . The relatively short length of the narrow probe appears to allow only a few minutes of undisturbed measurements before a thermal disturbance is conducted down from the larger diameter section above, limiting the accuracy of temperature extrapolations to about $\pm 0.1^{\circ}$ to 0.2°C under ideal conditions. In addition, the exact depth of penetration of the tool is never known with a certainty better than 1 to 2 m. From the shape of the temperature-time records and from comparison with nearby measurements, it is often possible to determine if the tool was pressed into fill at the bottom of a hole or if the formation cracked upon its insertion.

APC Tool Temperature Measurements

The APC heat-flow coring shoe is used for measuring in situ sediment temperatures during regular piston-coring operations. The instrument contains an electronics section that comprises three circuit boards and two battery packs, built into a cylindrical frame (Shipboard Scientific Party, 1992). The frame fits inside an annular cavity in a special coring shoe. Two steel prongs extend from the base of the frame to anchor the electronics in place inside the shoe. Inside one of the two prongs is a platinum resistance-temperature device (RTD) that has been calibrated over a range of -20° to 100°C . Along with the WSTP thermistors, five APC tools were calibrated at the WHOI facility in spring 1993 to provide absolute accuracy of about 0.005°C over a range of 0° to 35°C . Unlike the WSTP thermistor calibrations, those for the APC tool included the complete tool, sensor, battery, A/D, and data logger. The digital resolution is 0.05°C . The RTD prong is coated with thermally conductive grease to assure a good contact with the wall of the cutting shoe. As with the WSTP, the APC tool is not left in the sediments for a long enough time to achieve complete equilibration. Extrapolation of the data is described below, and results in an estimated in situ temperature with an accuracy of $\pm 0.05^{\circ}$ to 0.10°C under ideal conditions.

The tool is programmed after it has been inserted into the coring shoe, and repeated deployments can be run without removing the tool or batteries. The tool contains a microprocessor and 32 kilobytes of nonvolatile memory, and is run off a PC through an interface box. The tool operating system is downloaded from the computer, and the user defines a table of events, which includes the measurement frequency and total time of operation. During Leg 156, data generally were collected at a 5-s time interval. Between individual measurements, and optionally for extended periods, the tool can be programmed to "sleep" to conserve power.

After programming and starting the test sequence, a crossover sub-assembly with O-rings seals the cavity containing the electronics. The shoe is then placed at the front end of a core barrel and lowered down the drill pipe. The shoe is typically held just above the mud line to measure the temperature of bottom water, then lowered into the BHA. The

core barrel is deployed in the standard way, fired out through the bit using hydraulic pressure from the rig pumps, but it is left in place for 10 min, instead of being retrieved immediately, so that the tool can begin thermal equilibration with the formation. After the core barrel is returned to the ship, the coring shoe is removed and the temperature data are uploaded to the PC for reduction.

Data Reduction

Although the WSTP and APC tools have different geometries, the methods used for analyzing recovered temperature data are similar. For the WSTP, the thermal response of a cylindrical probe to a pulse of heating (or cooling) is given by Bullard (1954). The equivalent theory for the concentric cylinders and cylindrical shells of the APC tool is discussed by Horai and Von Herzen (1985). For both instruments, synthetic type-curves are constructed based on tool geometry, sampling interval, and the thermal properties of the tools and surrounding sediments. Both tools have thermal time constants of several minutes under normal conditions, which requires that the probes be kept in bottom for at least 10–15 min to allow extrapolation of the temperature curves with confidence.

The theoretical decay curves simulate the instantaneous heating (or cooling) of the sediment following probe penetration; however, in practice, a finite time is required for the sensors to reach a maximum temperature. As a result, the effective origin time of the thermal pulse is delayed as a function of tool and sediment properties. In addition, the recorders sample temperatures at fixed intervals, leaving the exact penetration time uncertain. An effective penetration time and an extrapolated temperature are estimated by shifting the time axis of the theoretical thermal decay curves to fit the actual data. Temperatures from the first 5 to 10 measurements (20–50 s) following penetration commonly do not follow the theoretical curves, but later parts of the records usually provide a close fit (Shipboard Scientific Party, 1992). The choice of which data should be included in the fitting, and which time shift should be used, is partly subjective. It is probably best to use as much of the actual decay curve as possible, particularly the early part of the record, as the theoretical functions have $1/t$ terms and thus favor later data during curve fitting. The variations in extrapolated temperatures that result from choosing different time intervals and time shifts can be used to estimate uncertainties associated with the temperatures finally assigned to represent in situ conditions.

VERTICAL SEISMIC PROFILING

Scientific Objectives

Vertical seismic profiling (VSP) experiments were planned so as to (1) determine the detailed *P*-wave velocity-depth structure of the drilled section, (2) determine the shear-wave structure near the décollement at Site 949, and (3) provide an accurate correlation between the drilled section and the regional three-dimensional seismic reflection data. An important component of the Leg 156 VSP program was to calibrate the "seismic" décollement by determining its thickness and velocity using a surface seismic source and down-hole receivers. VSP measurements provide such seismic information only for the interfaces penetrated by the borehole; reflecting interfaces below the bottom of the borehole are imaged by the VSP technique, but neither interval velocities nor time-depth information can be obtained (Gal'perin, 1974).

Acquisition Hardware

Leg 156 was the first deployment by ODP of Schlumberger's array seismic imager (ASI) for VSP acquisition. The ASI consists of an array of five seismic shuttles, each containing three orthogonal geophone accelerometers. The shuttles are spaced at 15.24-m intervals and are linked by a bridle to a signal-conditioning cartridge. The shuttles clamp magnetically to the casing. Each shuttle is equipped with a shaker

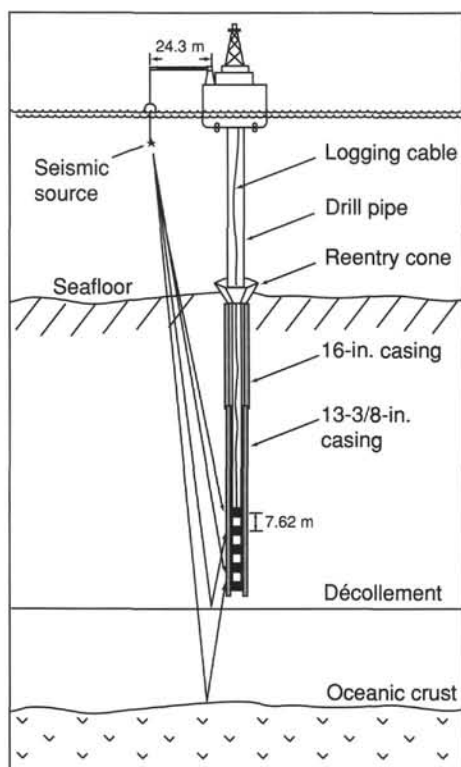


Figure 15. Diagram of zero-offset VSP experiment.

element that allows real-time evaluation of the coupling condition between the sensor package and the casing. The quality of the coupling between the casing and the surrounding sediment affects the quality of the signals recorded by the ASI. To check the degree of coupling, a cement-bond logging tool was run in the casing prior to deployment of the ASI (see "Downhole Logging" section, this chapter).

The signals received by the ASI were recorded in digital log interchange standard (DLIS) format on 4-mm (DAT) tape with the Schlumberger MAXIS system. DLIS tapes were then converted to SEGY, the standard seismic data format, using Schlumberger's LOGOS software. Initial onboard processing followed a standard sequence (e.g., Hardage, 1983), and was accomplished with Landmark's INSIGHT seismic-processing software on a computer workstation.

Zero-offset VSP

The clamping depth interval between geophones used for zero-offset VSP was 7.62 m. This depth interval allowed us to record unaliased frequencies as high as 100 Hz (the maximum frequency expected for an air-gun source) for velocities as low as 1524 m/s (the minimum velocity expected for the prism sediments). The seismic source for the zero-offset VSP experiments was an array of two Bolt 1500-C air guns suspended from a buoy at a water depth of about 7 m (Fig. 15). One air gun had a 4.9-L (300-in.³) chamber and one had a 2.0-L (120-in.³) chamber. A hydrophone suspended between the two guns was used to determine the shot-firing times (Fig. 16). The relative timing of the two guns was controlled by the Schlumberger MAXIS system. A second hydrophone suspended approximately 100 m below the ship was used to record the air-gun waveform for each shot. Seven to 15 shots were fired at each clamping level and summed to increase signal-to-noise levels. Four seconds of 1-ms data were recorded for each shot.

Ocean-bottom-shot VSP

Our main goal was to record shear waves and to detect shear-wave splitting, the most sensitive indicator of seismic anisotropy. The align-

ment of pore space and mineral grains ("scaly fabric") associated with the décollement zone are seismically anisotropic, as seen in core measurements. Above the décollement, the sediment is subject to lateral and vertical stresses and loses water throughout its thickness, along aligned pores that may cause seismic anisotropy. Shear-wave splitting is particularly sensitive to the volume, fluid pressure, and aspect ratio of aligned pores. We hoped to associate dilatant aligned pores with the high negative reflectance of the seismic décollement reflector at the borehole (Shipley et al., 1994).

Experiment Design Principles

Recording shear-wave shots downhole has two advantages over surface recording: (1) the formation of interest is the last part of the raypath from shot to receiver, so that the effects of formation anisotropy will be the most clearly seen, and (2) downhole recording avoids the undesirable effects of the sediment/water interface on shear waves (Liu et al., 1990; Liu and Crampin, 1990; Booth and Crampin, 1985).

We wanted to detect "shear-wave singularities," that is, directions of propagation in which the split shear waves have equal velocities and so are not effectively split. The exact directions in which these singularities occur is very sensitive to crack aspect ratio (Bush and Crampin, 1991). Raypaths close to shear-wave singularities are recognized in polarization diagrams (hodographs), as the motion is linear, rather than elliptical or cruciform (Crampin, 1991). The polarization of the faster split shear wave is usually different on either side of the singularity.

The optimal shot locations for detecting shear-wave singularities would be along radial lines at a range of azimuths to cover a range of incidence angles to the receivers. The most useful shear-wave singularities occur in directions neither parallel nor perpendicular to the directions of anisotropic symmetry. In the accretionary complex, the symmetry axis is probably east-west, the direction of horizontal plate motion.

Ocean-bottom Shots

Ocean-bottom explosive shots (Kirk et al., 1991) generated shear waves of a frequency of about 20 Hz when used in the January 1993 seismic survey of the drill sites. These have wavelengths of less than 50 m if the shear-wave velocity is less than 1 km/s.

Each shot used during Leg 156 consisted of four 2.7-kg (5-lb) cylinders of cast pentolite, wound with detonator cord and fitted into a weighted plastic cylinder. Just before deployment, an electrical detonator was inserted into the cylinder and connected to 150 m of cable. The shot was then deployed overboard from the starboard side of the fantail and the cable paid out. Only then was the cable connected to a canister that contained an electronic timer. The shot and timer were then allowed to fall to the seafloor. The falling time is about 25 min at an estimated terminal velocity of 3.3 m/s. The shots were pre-set to detonate after 24 hr.

Data were recorded on the Schlumberger MAXIS system. We used a digital sample interval of 2 ms to capture the *P*-wave and water wave; the MAXIS software allowed a recording window of only 32 s at this sample interval. One hydrophone was also connected to a continuous chart recorder, to confirm shot detonation.

PACKER EXPERIMENTS

Formation bulk permeability was measured at Sites 947 and 948 using a resettable drill-string packer manufactured by TAM International and described by Becker (1986, 1988). The packer incorporates inflatable rubber elements to isolate a section of the hole and can be configured as a single or a straddle packer. For the measurements during Leg 156, it was configured with one element and used as a single-seal packer to isolate the zone between the bottom of the hole and the seal or between the bottom of the hole and the deepest cementing point above (Fig. 17).

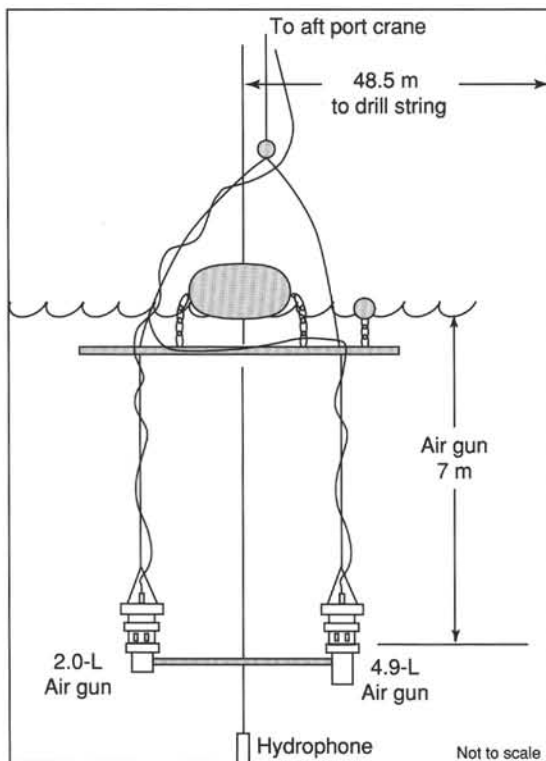


Figure 16. Air-gun configuration for zero-offset VSP experiment.

The packer is actuated using a “go-devil” that is dropped down the drill string into the packer inflation subassembly. The go-devil also carries recorders to monitor downhole fluid pressures in the isolated, pressurized zone during the experiment; these pressures are the primary data from which permeability is calculated. Two types of pressure recorders were used during Leg 156: (1) mechanical K-3 gauges made by Kuster Company, and (2) electronic ERPG-300 gauges made by Geophysical Research Corporation. The K-3 gauges record analog pressure mechanically by scratching a metal chart; the ERPG-300 gauges record in electronic memory digital pressure values sampled at 10.8-s intervals. The data from these gauges are not available until the go-devil is retrieved upon completion of the experiment. However, the entire drill string as well as the isolated zone was pressurized during testing, and a pressure transducer at the rig floor was also used to provide a real-time indication of downhole events. Throughout the packer measurements, pumping rates and total volumes pumped were also measured at the rig floor.

Once the packer was inflated, two kinds of experiments were used to determine the permeability of the isolated interval: pressure pulse (or “slug”) tests and constant-rate flow tests. The methods used were similar to those described by Anderson and Zoback (1982), Hickman et al. (1984), Anderson et al. (1985), and Becker (1989, 1990, 1991) when conducting packer experiments in Holes 395A, 504B, and 735B during DSDP and ODP. Constant-rate-flow tests generally disturb the pressure field in the formation around the hole much more than pressure-pulse tests and thus were conducted after the pressure-pulse tests at appropriate inflation depths.

Pulse Test Procedures

The pulse tests were conducted following the methods for the “modified” slug test of Bredehoeft and Papadopoulos (1980), which is an adaptation of the slug test method of Cooper et al. (1967) and Papadopoulos et al. (1973) for formations having relatively low permeabilities. In the modified slug test, a short pressure pulse is applied to the fluid in the zone isolated by the packer, and the decay of this pulse

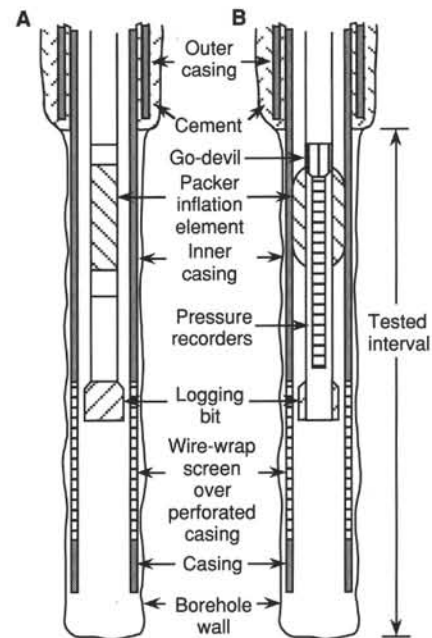


Figure 17. Sketch of the inflatable drill-string packer as deployed during Leg 156. **A.** The single-element packer incorporated in the BHA, before inflation or after deflation. **B.** Cut-away sketch of the inflated packer showing go-devil, pressure recorders, and tested, screened interval of the casing. During inflation of the packer, the go-devil directs fluids pumped from the rig floor into the inflation elements; once the packer is inflated, the go-devil position is shifted such that fluids pumped from the rig floor are directed into the tested interval.

is monitored as fluid flows from the borehole into the isolated formation. The decay of such a pressure pulse is described by the equation:

$$P(t)/P_0 = F(\alpha, \beta),$$

where $P(t)$ is pressure at time t , in excess of the initial undisturbed value; P_0 is the initial pressure increase, α is a dimensionless parameter that depends on the storage coefficient (S) and porosity (ϕ) of the isolated formation, β is a dimensionless parameter that depends on the transmissivity (T) and permeability (k) of the formation, and F is an infinite integral. More specifically,

$$\alpha = \pi a^2 S / V_w C_w \rho_w g,$$

$$\beta = \pi T_t / V_w C_w \rho_w g,$$

$$S = b \phi C_i \rho_i g, \text{ and}$$

$$T = b k \rho_i g / \mu,$$

where g is gravitational acceleration, a is the radius of the hole in the isolated zone, b is the vertical thickness of the isolated zone, C_i , ρ_i , and μ are, respectively, the compressibility, density, and dynamic viscosity of the fluid in the isolated zone, and C_w and ρ_w are the compressibility and density of the fluid in the total pressurized volume V_w .

The standard approach to processing pressure data measured during slug tests involves a curve-fitting method (Cooper et al., 1967; Papadopoulos et al., 1973) as follows. A plot of the decay of measured pressures vs. log time is superposed on a family of type curves of $F(\alpha, \beta)$ vs. log β calculated for various values of α spanning several orders of magnitude. The data plot is then shifted along the abscissa of the type-curve plot to determine visually the value of α for which the data best fit the type curve. Then the transmissivity and average permeability of the tested interval are calculated from the correspondence between the values of time and β for the best-fit curve, using the definitions for β and transmissivity given above.

As noted by Cooper et al. (1967), Papadopoulos et al. (1973), Bredehoeft and Papadopoulos (1980), and Hickman et al. (1984), the calculated type curves are relatively insensitive to changes in α and much more sensitive to changes in β . Thus, this procedure yields relatively poor estimates of the storage coefficient and porosity, but reasonable determinations of transmissivity and bulk permeability.

Constant-rate Flow Tests

In a relatively permeable formation, a pulse test will decay rapidly, and a better determination of permeability can be obtained by conducting a constant-rate flow test. In this experiment, borehole pressure within the isolated zone is monitored as fluids are pumped into the formation at a constant rate. The rise of pressure as injection proceeds quickly becomes linear with the log of time, according to the following equation (Horner, 1951; Matthews and Russell, 1967):

$$P(a,t) = (q\mu/4\pi kb)\ln(\tau\phi\mu C_a^2/4kt),$$

where q is the flux of injected fluids, τ is Euler's constant, and the remaining parameters are defined above. The average permeability of the isolated zone can be determined directly from the slope of a plot of pressure vs. log time, given the measured constant injection rate.

Properties of Fluids in a Pressurized System

The transient pressures measured during both slug and injection tests depend on the properties of the pressurized fluids, particularly viscosity and compressibility, which vary with both temperature and pressure. For the temperature-dependent viscosity of seawater, we used Gartling's (1977) equation, $\mu(10^{-3} \text{ Pa s}) = 16.68T^{-0.8987}$, with T in $^{\circ}\text{C}$, supplemented by steam-table data at temperatures below 10°C . As noted by Neuzil (1982), the effective compressibility of the fluid in a shut-in hole is sometimes greater than that of the pure fluid (seawater in this case), because of (1) compliance of the drill string and test equipment and (2) air trapped in the system. While every effort was made during Leg 156 to purge all air from the drill string, pump, and connecting plumbing, small amounts of air may have remained in the system. Such trapped air would increase the effective system compressibility and cause the transmissivity and bulk permeability calculated in a slug test to be erroneously high. Therefore, we carefully recorded the volumes pumped downhole during slug tests, so that the effective compressibility of the pressurized system could be determined using the definition of compressibility, $C = dV/VdP$, and could be accounted for when calculating the formation permeability.

Casing and Screen Configuration

Perforated and screened sections of casing were deployed at Sites 948 and 949 to keep the holes open for testing. Within the tested zones, the casing had a diameter of 27.3 cm and was perforated with 1.11 cm diameter holes at 1280 holes per meter of casing length. This configuration lead to 14.5% open area for the perforated casing. A wire-wrap screen was attached to the outside of the perforated casing. The wire had a diameter of 2.25 mm and was attached with a gap between wraps of 0.20 mm, providing about 8% open area. Between the perforated casing and wire screen were vertically welded, 3.18 mm steel rods. The use of these rods reduced the effective open area of the screen to about 6%, but the stand-off allowed the effective open area of the screen and perforated casing to be 6%, rather than the product of the casing and screen open areas, which would have been <2%. An open area of 6% is sufficient to maintain laminar flow conditions with the pumping rates used during packer testing.

LONG-TERM BOREHOLE OBSERVATORIES

Long-term borehole observatories (CORKs) were deployed at Sites 948 and 949 to monitor formation temperatures and pressures over several years following Leg 156. CORKs have been deployed

during two previous ODP cruises, Legs 139 and 146 (Davis, Mottl, Fisher, et al., 1992; Westbrook, Carson, Musgrave, et al., 1994). The conceptual and physical designs of the CORK system are described in detail in Davis et al. (1992); a short overview is provided here.

The CORK system comprises a modified reentry cone, a hydrologic seal that fits inside the throat of the cone, a data logger having sufficient power and memory to record data for about 2–3 yr, one or more pressure sensors situated below the seal plus an additional sea-floor sensor positioned above the seal, a sensor string including 10 or more thermistors hanging below the seal, and a valve mechanism by which the sealed hole can be vented to the overlying ocean. The hardware for forming the hydraulic seal and deploying the equipment was designed and constructed by the Engineering and Operations Group of the ODP science operator at Texas A&M University. Data loggers, sensor strings, and assorted fluid-sampling equipment are provided by third-party scientists. Two kinds of sensor strings and data loggers were deployed during Leg 156, one a modified version of the U.S./Canadian assembly deployed during Legs 139 and 146, and a new French assembly developed by scientists from the Institut Français de Recherche pour l'Exploitation de la Mer (IFREMER). The configuration of the cased and screened boreholes, the locations of thermistor and pressure sensors, and deployment operations for these instruments are described in the "Operations" sections of the appropriate site chapters. No scientific data collected as part of the CORK experiments were available during Leg 156.

The U.S./Canadian string deployed at Site 949 is similar to those deployed during previous legs, with slight modifications. The thermistor string hung below the Site 949 CORK comprises double braids of Kevlar around 10 pairs of conducting wires and a Kevlar strength member (see fig. 6 in the "Operations" section of "Site 949" chapter, this volume, for specific locations). Thermistor breakouts were woven into the string during its construction, along with slightly larger diameter outer Kevlar wraps at the breakouts. Polyethylene tubing of 0.5-in. diameter was pushed under the outer Kevlar weave in these locations, and thermistors were attached to the broken-out leads and pushed inside the tubing, then taped tightly to form a smooth transition with the surrounding cable. The Leg 156 U.S./Canadian cable also included two pressure transducers, one just below and one just above the hydraulic seal between the data logger pressure case and the CORK; earlier U.S./Canadian strings included only a single pressure transducer below the data logger. Finally, no fluid-sampling tubing was attached to the valve that connected the sealed borehole to the overlying ocean. Instead, taped to the Site 949 sensor string was a continuously operating osmotic sampler, described in the "Fluid Geochemistry" section (this chapter). In the U.S./Canadian sensor string, each sensor communicates with the data logger through one or more pairs of dedicated leads.

In contrast, the French sensor string deployed at Site 948 used two serial lines to communicate digitally between sensors and the data logger. This string comprises 20 sensor modules, 17 with two temperature sensors and three with one pressure and one temperature sensor. As with the U.S./Canadian string, the sensors in the French string are irregularly distributed along its length. The pressure sensors in the French string are located at the top, bottom, and in the middle of the string (see fig. 5 in the "Operations" section of "Site 948" chapter, this volume, for specific locations). Unlike the U.S./Canadian string, the French string can be shortened or lengthened at sea by removing or installing modules or sections of cable. The French string is configured such that every other sensor module is connected serially. Thus, if one of the lines stops operating, data still would be collected along the length of the string, albeit with half the spatial resolution. In contrast, the U.S./Canadian string contains 10 separate thermistor circuits. If one is disrupted, the other nine should continue to operate normally. The French string uses platinum resistance-temperature devices (nominally 1000 Ω at 0°C) as temperature sensors, while the U.S./Canadian string uses thermistors having a nominal resistance of 1 M Ω at 0°C .

The data loggers above both strings are programmed to record measurements once per hour. The U.S./Canadian logger has a memory capacity of 1 megabyte, while the French logger can store 4 megabytes. Both instruments are accessed electronically through an RS232 "wet connect" at the top of the pressure case. Once communication is established by a submersible or remotely operated vehicle (ROV), data can be downloaded and/or the loggers can be reprogrammed. Lithium batteries in both tools should allow data to be collected for at least 2 yr, and integrity of data to be maintained for at least 3 yr. Acoustic modems with separate power supplies may be attached to the data loggers during the first post-Leg 156 visit to the CORK sites so that the instruments can be accessed during subsequent expeditions without a submersible or ROV.

REFERENCES*

- Anadrill-Schlumberger, 1993. *Logging While Drilling*, document SMP-9160: Houston (Schlumberger).
- Anderson, R.N., and Zoback, M.D., 1982. Permeability, underpressures, and convection in the oceanic crust near the Costa Rica Rift, eastern equatorial Pacific. *J. Geophys. Res.*, 87:2860–2868.
- Anderson, R.N., Zoback, M.D., Hickman, S.H., and Newmark, R.L., 1985. Permeability vs. depth in the upper oceanic crust: in situ measurements in DSDP Hole 504B, eastern equatorial Pacific. *J. Geophys. Res.*, 90:3659–3669.
- ASTM, 1989. *Annual Book of ASTM Standards for Soil and Rock, Building Stones: Geotextiles* (Vol. 04.08): Philadelphia (Am. Soc. Testing Materials).
- Barnes, R.O., 1979. Operation of the IPOD in-situ pore water sampler [in "Introduction and Explanatory Notes" chapter]. In Sibuet, J.-C., Ryan, W.B.F., et al., *Init. Repts. DSDP*, 47 (Pt. 2): Washington (U.S. Govt. Printing Office), 19–22.
- Barnes, R.O., 1988. ODP in-situ fluid sampling and measurement: a new wireline tool. In Mascle, A., Moore, J.C., et al., *Proc. ODP, Init. Repts.*, 110: College Station, TX (Ocean Drilling Program), 55–63.
- Becker, K., 1986. Special report: development and use of packers in ODP. *JOIDES J.*, 12:51–57.
- , 1988. A guide to ODP tools for downhole measurements. *ODP Tech. Note*, 10.
- , 1989. Measurements of the permeability of the sheeted dikes in Hole 504B, ODP Leg 111. In Becker, K., Sakai, H., et al., *Proc. ODP, Sci. Results*, 111: College Station, TX (Ocean Drilling Program), 317–325.
- , 1990. Measurements of the permeability of the upper oceanic crust at Hole 395A, ODP Leg 109. In Detrick, R., Honnorez, J., Bryan, W.B., Juteau, T., et al., *Proc. ODP, Sci. Results*, 106/109: College Station, TX (Ocean Drilling Program), 213–222.
- , 1991. In-situ bulk permeability of oceanic gabbros in Hole 735B, ODP Leg 118. In Von Herzen, R.P., Robinson, P.T., et al., *Proc. ODP, Sci. Results*, 118: College Station, TX (Ocean Drilling Program), 333–347.
- Behrmann, J.H., Lewis, S.D., Musgrave, R.J., et al., 1992. *Proc. ODP, Init. Repts.*, 141: College Station, TX (Ocean Drilling Program).
- Bergen, J.A., 1984. Calcareous nannoplankton from Deep Sea Drilling Project Leg 78A: evidence for imbricate underthrusting at the Lesser Antillean active margin. In Biju-Duval, B., Moore, J.C., et al., *Init. Repts. DSDP*, 78 (Pt. 1): Washington (U.S. Govt. Printing Office), 411–445.
- Blum, P., 1994. Index properties, vers. 155. In *ODP Shipboard Laboratory Manual*: College Station, TX (Ocean Drilling Program).
- Bolli, H.M., and Saunders, J.B., 1985. Oligocene to Holocene low latitude planktic foraminifera. In Bolli, H.M., Saunders, J.B., and Perch-Nielsen, K. (Eds.), *Plankton Stratigraphy*: Cambridge (Cambridge Univ. Press), 155–262.
- Booth, D.C., and Crampin, S., 1985. Shear wave polarizations on a curved wavefront at an isotropic free-surface. *Geophys. J. R. Astron. Soc.*, 83:31–45.
- Boyce, R.E., 1976. Definitions and laboratory techniques of compressional sound velocity parameters and wet-water content, wet-bulk density, and porosity parameters by gravimetric and gamma ray attenuation techniques. In Schlanger, S.O., Jackson, E.D., et al., *Init. Repts. DSDP*, 33: Washington (U.S. Govt. Printing Office), 931–958.
- Bredheoef, J.D., and Papadopoulos, S.S., 1980. A method for determining the hydraulic properties of tight formations. *Water Resour. Res.*, 16:223–238.
- Bukry, D., 1973. Low-latitude coccolith biostratigraphic zonation. In Edgar, N.T., Saunders, J.B., et al., *Init. Repts. DSDP*, 15: Washington (U.S. Govt. Printing Office), 685–703.
- , 1975. Coccolith and silicoflagellate stratigraphy, northwestern Pacific Ocean, Deep Sea Drilling Project Leg 32. In Larson, R.L., Moberly, R., et al., 32: Washington (U.S. Govt. Printing Office), 677–701.
- Bullard, E.C., 1954. The flow of heat through the floor of the Atlantic Ocean. *Proc. R. Soc. London A*, 222:408–429.
- Bush, I., and Crampin, S., 1991. Paris Basin VSPs: case history establishing combinations of matrix- and crack-anisotropy from modelling shear wavefields near point singularities. *Geophys. J. Int.*, 107:433–447.
- Cande, S.C., and Kent, D.V., 1992. A new geomagnetic polarity time scale for the Late Cretaceous and Cenozoic. *J. Geophys. Res.*, 97:13917–13951.
- Clark, M.W., 1990. Cenozoic calcareous nannofossils from the Lesser Antilles Forearc region and biostratigraphic summary of Leg 110. In Moore, J.C., Mascle, A., et al., *Proc. ODP, Sci. Results*, 110: College Station, TX (Ocean Drilling Program), 129–140.
- Cook, H.E., Johnson, P.D., Matti, J.C., and Zemmels, I., 1975. Methods of sample preparation and X-ray diffraction data analysis, X-ray Mineralogy Laboratory, Deep Sea Drilling Project, University of California, Riverside. In Hayes, D.E., Frakes, L.A., et al., *Init. Repts. DSDP*, 28: Washington (U.S. Govt. Printing Office), 999–1007.
- Cooper, H.H., Jr., Bredheoef, J.D., and Papadopoulos, I.S., 1967. Response of a finite diameter well to an instantaneous charge of water. *Water Resour. Res.*, 3:267–269.
- Crampin, S., 1991. Effects of singularities on shear-wave propagation in sedimentary basins. *Geophys. J. Int.*, 107:531–543.
- Davis, E.E., Becker, K., Pettigrew, T., Carson, B., and MacDonald, R., 1992. CORK: a hydrologic seal and downhole observatory for deep-ocean boreholes. In Davis, E.E., Mottl, M.J., Fisher, A.T., et al., *Proc. ODP, Init. Repts.*, 139: College Station, TX (Ocean Drilling Program), 43–53.
- Davis, E.E., Mottl, M.J., Fisher, A.T., et al., 1992. *Proc. ODP, Init. Repts.*, 139: College Station, TX (Ocean Drilling Program).
- Desbrandes, R., 1994. *Data Acquisition and Processing While Drilling*: Dept. Petrol. Eng., Louisiana State Univ.
- Espitalié, J., 1980. Role of mineral matrix in kerogen pyrolysis: influence on petroleum generation and migration. *AAPG Bull.*, 64:59–66.
- Espitalié, J., Deroo, G., and Marquis, F., 1985a. La pyrolyse Rock-Eval et ses applications, Partie I. *Rev. Inst. Fr. Pet.*, 40/5:563–579.
- , 1985b. La pyrolyse Rock-Eval et ses applications, Partie II. *Rev. Inst. Fr. Pet.*, 40/6:755–784.
- , 1986. La pyrolyse Rock-Eval et ses applications, Partie III. *Rev. Inst. Fr. Pet.*, 41:73–89.
- Fan, P.-F., and Rex, R.W., 1972. X-ray mineralogy studies—Leg 14. In Hayes, D.E., Pimm, A.C., et al., *Init. Repts. DSDP*, 14: Washington (U.S. Govt. Printing Office), 677–725.
- Fisher, A.T., and Hounslow, M.W., 1990. Heat flow through the toe of the Barbados accretionary complex. In Moore, J.C., Mascle, A., et al., *Proc. ODP, Sci. Results*, 110: College Station, TX (Ocean Drilling Program), 345–363.
- Gal'perin, E.I., 1974. *Vertical Seismic Profiling*. Spec. Publ.—Soc. Explor. Geophys., 12.
- Gartling, D.K., 1977. Convective heat transfer analysis by the finite element method. *Comput. Methods Appl. Mech. Eng.*, 12:365–382.
- Gartner, S., 1977. Calcareous nannofossil biostratigraphy and revised zonation of the Pleistocene. *Mar. Micropaleontol.*, 2:1–25.
- Gieskes, J.M., Gamo, T., and Brumsack, H., 1991. Chemical methods for interstitial water analysis aboard *JOIDES Resolution*. *ODP Tech. Note*, 15.
- Gillis, K., Mével, C., Allan, J., et al., 1993. *Proc. ODP, Init. Repts.*, 147: College Station, TX (Ocean Drilling Program).
- Hardage, B.A., 1983. *Vertical Seismic Profiling, Part A: Principles*: London (Geophysical Press).
- Hickman, S.H., Langseth, M.G., and Svitek, J.F., 1984. In situ permeability and pore-pressure measurements near the Mid-Atlantic Ridge, Deep Sea Drilling Project Hole 395A. In Hyndman, R.D., Salisbury, M.H., et al., *Init. Repts. DSDP*, 78B: Washington (U.S. Govt. Printing Office), 699–708.
- Hoppie, B., Blum, P., and Shipboard Scientific Party, in press. Natural gamma-ray measurements on ODP cores: Introduction to procedures with examples from Leg 150. In Mountain, G.S., Miller, K.G., Blum, P., et al., *Proc. ODP, Init. Repts.*, 150: College Station, TX (Ocean Drilling Program).

* Abbreviations for names of organizations and publication titles in ODP reference lists follow the style given in *Chemical Abstracts Service Source Index* (published by American Chemical Society).

- Horai, K., and Von Herzen, R.P., 1985. Measurement of heat flow on Leg 86 of the Deep Sea Drilling Project. In Heath, G.R., Burckle, L.H., et al., *Init. Repts. DSDP, 86*: Washington (U.S. Govt. Printing Office), 759–777.
- Homer, D.R., 1951. Pressure build-up in wells. *Proc. Third World Pet. Congr.*, 2:501.
- Hounslow, M.W., 1990. Grain fabric measured using magnetic susceptibility anisotropy in deformed sediments of the Barbados accretionary prism: Leg 110. In Moore, J.C., Mascle, A., et al., *Proc. ODP, Sci. Results*, 110: College Station, TX (Ocean Drilling Program), 257–275.
- Katz, B.J., 1983. Limitations of Rock-Eval pyrolysis for typing organic matter. *Org. Geochem.*, 4:195–199.
- Kirk, R.E., Robertson, K., Whitmarsh, R.B., and Miles, P.R., 1991. A technique for conducting seismic refraction experiments on the ocean bed using bottom shots. *Mar. Geophys. Res.*, 13:153–160.
- Liu, E., and Crampin, S., 1990. Effects of the internal shear-wave window: comparison with anisotropy induced splitting. *J. Geophys. Res.*, 95:11275–11281.
- Liu, E., Crampin, S., and Yardley, G., 1990. Polarizations of reflected shear waves. *Geophys. Res. Lett.*, 17:1137–1140.
- Lundberg, N., and Moore, J.C., 1986. Macroscopic structural features in Deep Sea Drilling Project cores from forearc regions. In Moore, J.C. (Ed.), *Structural Fabric in Deep Sea Drilling Project Cores From Forearcs*. Mem.—Geol. Soc. Am., 166:13–44.
- Maltman, A.J., Byrne, T., Karig, D.E., Lallemand, S., Knipe, R., and Prior, D., 1993. Deformation structures at Site 808, Nankai accretionary prism, Japan. In Hill, I.A., Taira, A., Firth, J.V., et al., *Proc. ODP, Sci. Results*, 131: College Station, TX (Ocean Drilling Program), 123–133.
- Manheim, F.T., and Sayles, F.L., 1974. Composition and origin of interstitial water of marine sediments based on deep sea drill cores. In Goldberg, E.D. (Ed.), *The Sea* (Vol. 5): New York (Wiley Interscience), 527–568.
- Mascle, A., Moore, J.C., Taylor, E., and Shipboard Scientific Party, 1988. ODP Leg 110 at the northern Barbados Ridge: introduction and explanatory notes. In Mascle, A., Moore, J.C., et al., *Proc. ODP, Init. Repts.*, 110: College Station, TX (Ocean Drilling Program), 5–25.
- Matthews, C.S., and Russell, D.G., 1967. *Pressure Build-up and Flow Tests in Wells*. Soc. Pet. Eng., AIME, Monogr. 1.
- Mayer, L.A., Courtney, R.C., and Moran, K., 1987. Ultrasonic measurements of marine sediment measurements of marine sediment properties. *Proc. Oceanog.*, 87:1–139.
- Mazzullo, J.M., Meyer, A., and Kidd, R.B., 1988. New sediment classification scheme for the Ocean Drilling Program. In Mazzullo, J., and Graham, A.G. (Eds.), *Handbook for Shipboard Sedimentologists*. ODP Tech. Note, 8:45–67.
- Neuzil, C.E., 1982. On conducting the modified “slug” test in tight formations. *Water Resour. Res.*, 18:439–441.
- Nigrini, C., 1971. Radiolarian zones in the Quaternary of the equatorial Pacific Ocean. In Funnell, B.M., and Riedel, W.R. (Eds.), *The Micropalaeontology of Oceans*: Cambridge (Cambridge Univ. Press), 443–461.
- Okada, H., and Bukry, D., 1980. Supplementary modification and introduction of code numbers to the low-latitude coccolith biostratigraphic zonation (Bukry, 1973; 1975). *Mar. Micropaleontol.*, 5:321–325.
- Papadopoulos, S.S., Bredehoeft, J.D., and Cooper, H.H., 1973. On the analysis of “slug test” data. *Water Resour. Res.*, 9:1087–1089.
- Peters, K.E., 1986. Guidelines for evaluating petroleum source rock using programmed pyrolysis. *AAPG Bull.*, 70:318–329.
- Pettijohn, E.J., Potter, P.E., and Siever, R., 1973. *Sand and Sandstone*: New York (Springer-Verlag).
- Pyle, M.R., 1984. Vane shear data on undrained residual strength. *J. Geotech. Engr. Div., Am. Soc. Civ. Eng.*, 110:543–547.
- Riedel, W.R., and Sanfilippo, A., 1978. Stratigraphy and evolution of tropical Cenozoic radiolarians. *Micropaleontology*, 24:61–96.
- Sanfilippo, A., Westberg-Smith, M.J., and Riedel, W.R., 1985. Cenozoic radiolaria. In Bolli, H.M., Saunders, J.B., and Perch-Nielsen, K. (Eds.), *Plankton Stratigraphy*: Cambridge (Cambridge Univ. Press), 631–712.
- Schlumberger, Inc., 1989. *Log Interpretation Principles/Applications*: Houston (Schlumberger).
- Serra, O., 1984. *Fundamentals of Well-Log Interpretation* (Vol. 1): *The Acquisition of Logging Data*: Amsterdam (Elsevier).
- Shepard, F.P., 1954. Nomenclature based on sand-silt-clay ratios. *J. Sediment. Petrol.*, 24:151–158.
- Shipboard Scientific Party, 1992. Explanatory notes. In Davis, E.E., Mottl, M.J., Fisher, A.T., et al., *Proc. ODP, Init. Repts.*, 139: College Station, TX (Ocean Drilling Program), 55–97.
- Shiple, T., Ogawa, Y., and Blum, P., 1994. Leg 156 scientific prospectus. *ODP Sci. Prospectus*, 56.
- Shiple, T.H., Moore, G.F., Bangs, N., Moore, J.C., and Stoffa, P.L., 1994. Seismically inferred dilatancy distribution, northern Barbados Ridge décollement: implications for fluid migration and fault strength. *Geology*, 22:411–414.
- Taira, A., Hill, I., Firth, J.V., et al., 1991. *Proc. ODP, Init. Repts.*, 131: College Station, TX (Ocean Drilling Program).
- Timur, A., and Toksöz, M.N., 1985. Downhole geophysical logging. *Annu. Rev. Earth Planet. Sci.*, 13:315–344.
- Von Herzen, R.P., and Maxwell, A.E., 1959. The measurements of thermal conductivity of deep-sea sediments by a needle-probe method. *J. Geophys. Res.*, 64:1557–1563.
- Westbrook, G.K., Carson, B., Musgrave, R.J., et al., 1994. *Proc. ODP, Init. Repts.*, 146 (Pt. 1): College Station, TX (Ocean Drilling Program).
- Yokota, T., Kinoshita, H., and Uyeda, S., 1980. New DSDP (Deep Sea Drilling Project) downhole temperature probe utilizing IC RAM (memory) elements. *Bull. Earthquake Res. Inst., Univ. Tokyo*, 55:75–88.

Ms 156IR-104